EXPERIENCES ON *p*-VERSION TIME-DISCONTINUOUS GALERKIN'S METHOD FOR NONLINEAR HEAT TRANSFER ANALYSIS AND SENSITIVITY ANALSYIS

Gene Hou

Department of Mechanical Engineering
Old Dominion University
Norfolk, VA 23529-0247

Abstract

The focus of this research is on the development of analysis and sensitivity analysis equations for nonlinear, transient heat transfer problems modeled by *p*-version, time discontinuous finite element approximation. The resulting matrix equation of the state equation is simply in the form of $A(x)x = c$, representing a single step, time marching scheme. The Newton-Raphson's method is used to solve the nonlinear equation. Examples are first provided to demonstrate the accuracy characteristics of the resultant finite element approximation. A direct differentiation approach is then used to compute the thermal sensitivities of a nonlinear heat transfer problem. The report shows that only minimal coding effort is required to enhance the analysis code with the sensitivity analysis capability.

I. Introduction

The *p*-version Galerkin's method with discontinuity in time developed here was based upon the work done by Bey and her colleagues[1-3]. The method uses hierarchical high-order polynomials to interpolate the temperature through the thickness of the panels. Therefore, the method can catch high thermal gradients without introducing geometrical discretization through thickness. This special feature of the method offers an order of reduction in finite element modeling. That makes the method very attractive to many engineering applications. Furthermore, the method treats time as the fourth dimension in its discretization and formulation. The weak continuity condition is imposed at the joints between each time intervals (or elements). The end result is a high order, single step time marching scheme. Though the stability of the method is ensured, the error analysis and the adaptivity of the method have been the focus of recent research.

The emphases of the work reported here are placed upon the numerical modeling of temperature-dependent and distributive nature of material properties. Such approximation not only affects the accuracy of the analysis but also the formation of Jacobian matrices which are required in the Newton-Raphson's method and sensitivity analysis. Numerical examples are provided to show the relations between the modeling parameters and the accuracy of the method. An attempt is also made to analyze a heat conduction problem with a moving heat source.

Sensitivity analysis is defined in this report as a process that derives sensitivity equations to compute the derivatives of responses or states with respect to specified variables. Since the derivative information can greatly enhance the robustness and accuracy of curve fitting, sensitivity analysis becomes a necessary element in many engineering applications; such as design trade-off, weather prediction, analysis error correction, model adjustment, reliability analysis and design optimization. It is shown that the sensitivity equation can be derived and solved using the direct differentiation method with a minimal effort in the framework of *p*-version Galerkin's method with discontinuity in time. The design variables used in this study are related to material distribution. The applications of such derivatives are also briefly discussed in the report.

The report is organized as follows. Section II details the *p*-version Galerkin's formulation. Section III discusses the construction and the solution strategies of the required finite element equations. Section IV derives sensitivity equations based upon the direct differentiation strategy. Section V reports the results of numerical studies. Concluding remarks are given at the end of the report. Some of the results have been published as a proceeding paper in the 14th Annual Thermal and Fluids Analysis Workshop, August 18th to 22nd, 2003 in Hampton, VA. The paper is listed as the first attachment of the report. The computer code developed in this study, along with the input of a 3D example, is attached in a CD.

II. *p*-Version, Time-Discontinuous Galerkin's Method

The governing differential equation of a general heat conduction problem is given as

$$\rho c\frac{\partial u}{\partial t}-\sum_{i=1}^{3}\sum_{j=1}^{3}\frac{\partial}{\partial x_i}\left[k_{ij}\frac{\partial u}{\partial x_j}\right]=Q(x,t),\quad \text{in}\ \ \Omega\times(0,T] \tag{1}$$

$$u=f(x,t) \qquad \text{on}\ \ \partial\Omega_u\times(0,T] \tag{2}$$

$$\sum_{i=1}^{3}\sum_{j=1}^{3}k_{ij}\frac{\partial u}{\partial x_j}[n_i]=q_s(x,t), \qquad \text{on}\ \ \partial\Omega_q\times(0,T] \tag{3}$$

$$\sum_{i=1}^{3}\sum_{j=1}^{3}k_{ij}\frac{\partial u}{\partial x_j}[n_i]=-h(u-T_\infty), \qquad \text{on}\ \ \partial\Omega_h\times(0,T] \tag{4}$$

and

$$u=g(x), \qquad \text{in}\ \ \Omega\ \text{at}\ t=0 \tag{5}$$

where the temperature, u(x,t), is the only unknown. Equation 1 represents an initial-boundary value problem with Eqs.(2-4) being the temperature and the heat flux boundary conditions, and the thermal convective condition; respectively, and Eq. (5), the initial conditions. It is assumed that the heat source, Q, the prescribed

temperature, f, the flux, q_s, the thermal film coefficient, h, and the initial value, g, are all with proper regularity. In case of material nonlinearity, the specific heat, ρc(u), the film coefficient, $h(u)$, and the thermal conductivity, k_{ij}(u) are assumed to be functions of temperature.

Let $f = 0$ on Ω_u. Otherwise, u in Eqs.(1-5) can be replaced by $u - f$ to achieve a homogenous boundary condition on Ω_u. As a result, the weak form of Eqs. (1-5) can be derived, based upon the Galerkin's Method for an arbitrary function, $w(x)$, as

$$\int_{\Omega}(\rho c\frac{\partial u}{\partial t}w+\sum_{i=1}^{3}\sum_{j=1}^{3}k_{ij}\frac{\partial u}{\partial x_i}\frac{\partial w}{\partial x_j})dv+\int_{\partial\Omega_h}huwds$$

$$=\int_{\Omega}Qwdv+\int_{\partial\Omega_q}q_s wds+\int_{\partial\Omega_h}hT_\infty wds \tag{6}$$

In the approach of time-discontinuous Galerkin's method, the time coordinate is treated as the same as the spatial coordinate. The time space is also discretized into elements or intervals. Focusing on one time interval, $I_n = [t_{n-1}, t_n)$, the weak form, Eq. (6), can be extended to the entire product domain $\Omega \times I_n$

$$\int_{n-1}^{n}[\int_{\Omega}\rho c\frac{\partial u}{\partial t}w+\sum_{i=1}^{3}\sum_{j=1}^{3}k_{ij}\frac{\partial u}{\partial x_i}\frac{\partial w}{\partial x_j})dv]dt+\int_{n-1}^{n}[\int_{\partial\Omega_h}huwds]dt$$

$$=\int_{n-1}^{n}[\int_{\Omega}Qwdv+\int_{\partial\Omega_q}q_s wds+\int_{\partial\Omega_h}hT_\infty wds]dt \tag{7}$$

where, $w(x,t)$ is the testing function. Furthermore, to enforce the continuous requirement at the interface of the time interval at t_{n-1}, a weighted integral form of a constraint is imposed to Eq. (7) as

$$\int_{\Omega}(\rho c^{+}u^{+}-\rho c^{-}u^{-})w^{+}dv=0 \tag{8}$$

which is a weak form of the jump condition, $\rho^{+}_{n-1}c^{+}_{n-1}w^{+}_{n-1}=\rho^{-}_{n-1}c^{-}_{n-1}w^{+}_{n-1}$, at t_{n-1}, where

$$u^{-}_{n-1}=\lim_{\varepsilon\to 0}u(x,t_{n-1}-\varepsilon)$$

$$u^{+}_{n-1}=\lim_{\varepsilon\to 0}u(x,t_{n-1}+\varepsilon)$$

and other variables with the superscripts "+" and "-" and the subscript "$n-1$" have similar definitions. Note that $\rho^{-}_{n-1}c^{-}_{n-1}$ is evaluated at t_{n-1} in I_{n-1}, whereas $\rho^{+}_{n-1}c^{+}_{n-1}$ *and* w^{+}_{n-1} are evaluated at the same time instant, t_{n-1}, but in I_n.

III. Finite Element Equations and Solution Strategy

The domain of an triangular element is defined as $\Omega_e \times I_n$, which Ω_e can be further divided into two spaces; $\Omega_p(x,y)$ and $\Omega_d(z)$, where *(x, y, z)* is within a triangle bounded by three vertices $(x_i,y_i),(x_j,y_j)$,and (x_k,y_k) and $\frac{-d}{2} \le z \le \frac{d}{2}$ where *d* is the thickness. The non-dimensional local coordinates selected to represent *(x,y)*, *z*, and *t* are defined by the area coordinates (L_i,L_j,L_k), and non-dimensional variables, ξ and τ ,respectively, where

$$x = L_i x_i + L_j x_j + L_k x_k$$
$$y = L_i y_i + L_j y_j + L_k y_k$$
$$1 = L_i + L_j + L_k,$$

and

$$\xi = \frac{2z}{d}$$
$$\tau = \frac{2(t - t_{n-1})}{t_n - t_{n-1}} - 1$$

The solution, $u_n = u(x,y,z,t)$ in an element, $\Omega_p \times \Omega_d \times I_n$, is interpolated in terms of $\phi_i(L_i,L_j,L_k),\psi(\xi)$ and $\theta_k(\tau)$ as

$$u_n = \sum_{i=1}^{I_p} \sum_{j=1}^{I_d} \sum_{k=1}^{I_t} \phi_i \psi_j \theta_k a_{ijk}^n \tag{10}$$

or in a vector form

$$u_n(x,t) = \chi^T(x,y,z,t) a_n$$
$$= (\phi(x,y) \otimes \psi(z) \otimes \theta(t))^T a_n \tag{11}$$

where the symbol, $\otimes$, represents the outer tensor product operator and the vectors, ϕ, ψ and θ, represent collections of basis functions. Particularly, the through-thickness basis functions, ψ, are made of the Legendre polynomials of the first kind[1], the temporal basis functions, θ, the integrations of the same Legendre polynomials and the in-plane basis functions, ϕ, chosen for triangular elements, as described by Reference 4.

In Eq. (10), I_p, I_d and I_t represent the numbers of shape functions for planar triangular, through-thickness and through-time interpolation, respectively. In our case,

$$I_p = (3 + 3*(I_{pp} - 1) + (I_{pp} - 1)*(I_{pp} - 2)/2)$$
$$I_d = (I_{pd} + 1)$$
$$I_t = (I_{pt} + 1)$$

where I_{pp}, I_{pd} and I_{pt} are the orders of hierarchical polynomials used for interpolations. Particularly, in the planar space, there are 3 for vertex shape functions, $3*(I_{pp} - 1)$ for edge functions and $(I_{pp} - 1)*(I_{pp} - 2)/2$ for the interior bubble

functions. The details of the interpolation functions for temperature are listed in Appendices I to III.

It is assumed that in this study, the film coefficient h is set to zero and the relations between the other material properties, ρc and K_{ij}, and the temperature are defined in a tabulated form, presented as a result of experiments. Therefore, the material properties cannot be explicitly specified as functions of position and time as required by integration. An approximation is thus introduced to overcome such a difficulty. The standard Lagrange polynomials are used here for this purpose.

The values of the material properties at the Lagrange points are taken from a given material table based upon the values of the temperature found at those points. The values of the material properties at elsewhere in an element are then obtained through interpolation. In this way, the material properties can be explicitly approximated as functions of position and time throughout the problem domain. The detailed Lagrange polynomials are given in Appendices IV and V for interpolating material properties.

As an example, the material property, say ρc, can be interpolated in an element $(\Omega_p \times I_n)$ as

$$\begin{aligned} \rho c(x,t) &= (N_c(x,y,z,t))^T \delta_c \\ &= (N_{cp}(x,y) \otimes N_{cz}(z) \otimes N_{ct}(t))^T \delta_c \\ &= \sum_i \sum_j \sum_k (N_{cpi}(x,y) \otimes N_{czj}(z) \otimes N_{ctk}(t))^T \delta_{cijk} \end{aligned} \tag{12}$$

where, δ_{cijk} is a component of the vector, δ_c, which takes the value of the material properties found in the material table based upon the temperature evaluated at the point (x_i, y_i, z_j, t_k). Specifically, if the point is called point m, the temperature at point m, $T_m(x_i, y_i, z_j, t_k)$, is given as $T_m = \chi_m^T a_n$ where a_n is the unknown of the matrix equation in time interval, I_n, and $\chi_m = \varphi(x_i, y_i) \otimes \psi(z_j) \otimes \theta(t_k)$ evaluated at point m.

Since the code studied here considers the material properties are input in a tabulated form. And the relationship between the material properties and the temperature is expressed by a precisely linear function as shown in Fig. 2.1.

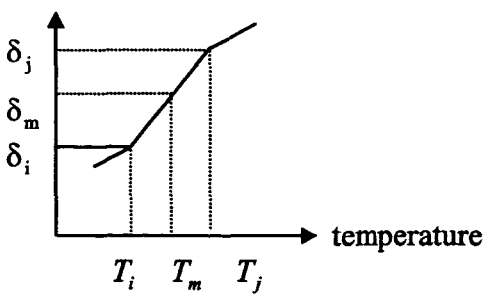

Figure 2.1. Material Property-Temperature Relation

Thus, if the calculated temperature, T_m, falls between a pair of given data points, $T_i \le T_m \le T_j$, the material value, δ_m, which represents δ_{cijk} in Eq. (12), is given as

$$\delta_m = \delta_i + (\frac{\delta_j - \delta_i}{T_j - T_i})(T_m - T_i)$$

or rewritten as

$$\delta_m = \frac{\delta_i(T_j - T_i) - T_i(\delta_j - \delta_i)}{T_j - T_i} + (\frac{\delta_j - \delta_i}{T_j - T_i})T_m$$
$$= (\frac{\delta_i T_j - T_i \delta_j}{T_j - T_i}) + \frac{(\delta_j - \delta_i)}{(T_j - T_i)} T_m$$

which can be abbreviated as

$$\delta_m = \beta_m + \alpha_m T_m$$

where

$$\beta_m = \frac{\delta_i T_j - T_i \delta_j}{T_j - T_i}$$
$$\alpha_m = \frac{(\delta_j - \delta_i)}{(T_j - T_i)}$$

Therefore, one has a linear relationship between the material property and the temperature,

$$\delta_m = \beta_m + (\alpha_m \chi_m)^T a_n \tag{13}$$

The differentiation of δ_m with respect to a_n is then obtained as a constant vector,

$$\frac{\partial \delta_m}{\partial a_n} = (\alpha_m \chi_m)^T \tag{14}$$

The above equation is needed in computing the Jacobian matrices for Newton-Raphson's iteration.

Once the interpolation functions are selected and the nonlinear material properties are approximated as explicit functions of position and time as shown in Eqs. (11-12), one can proceed to integrate the terms in Eqs.(7-8) to construct the equivalent matrices. The resultant finite element matrix equation for the time interval, I_n, can then be expressed as

$$[C_n(a_n) + K_n(a_n) + M_n^+(a_n)]a_n = q_n + [M_{n-1}^-(a_{n-1})]a_{n-1} + b_n \tag{15}$$

where the subscript, n, indicates that the associated matrix or vector is evaluated with functions defined in time interval, I_n. Note that each term in Eq.(15) is corresponding to an integral in Eqs.(7-8), which can be evaluated based upon the interpolation functions of Eqs. (11-12). As an example, the capacitance matrix is given as

$$C_n = \sum_p C_{\Omega_p}$$

$$= \sum_p \int_{t_{n-1}}^{t_n} \left(\int_{\Omega_n} \rho c \frac{\partial u}{\partial t} w dx \right) dt$$

The details of an elemental capacitance matrix, C_{Ω_p} and other related elemental matrices are given as Eq.(VI.1) in Appendix VI.

The matrix equation derived above is based upon the discontinuous Galerkin's method and will be solved in a time-marching fashion. In other words, the matrix equation of Eq.(15) will be solved for a time interval at a time, with $\boldsymbol{a}_n$ as unknown and $\boldsymbol{a}_{n-1}$ known quantities. Because of its nonlinear nature, Eq.(15) can be solved by the Newton-Raphson's method, which leads to a recursive formula

$$\begin{aligned} &[\boldsymbol{C}_n(\boldsymbol{a}_n^{i-1}) + \boldsymbol{K}_n(\boldsymbol{a}_n^{i-1}) + \boldsymbol{M}_n^+(\boldsymbol{a}_n^{i-1}) + \boldsymbol{J}_c(\boldsymbol{a}_n^{i-1}) + \boldsymbol{J}_k(\boldsymbol{a}_n^{i-1}) + \boldsymbol{J}_m(\boldsymbol{a}_n^{i-1})]\Delta\boldsymbol{a}_n^i \\ &= -\boldsymbol{R}_n^{i-1} \end{aligned} \tag{16}$$

and the unknown is updated by

$$\boldsymbol{a}_n^i = \boldsymbol{a}_n^{i-1} + \Delta\boldsymbol{a}_n^i \tag{17}$$

In the above equation, $\Delta\boldsymbol{a}_n^i$ is the improvement of the solution and $\boldsymbol{R}_n^{i-1}$ is the residual of the nonlinear equation at the i-1 iteration, which is defined as

$$\boldsymbol{R}_n^{i-1} = \left[C_n(\boldsymbol{a}_n^{i-1}) + K_n(\boldsymbol{a}_n^{i-1}) + M_n^+(\boldsymbol{a}_n^{i-1})\right]\boldsymbol{a}_n^i - \boldsymbol{q}_n - [M_{n-1}^-(\boldsymbol{a}_{n-1})]\boldsymbol{a}_{n-1} - \boldsymbol{b}_n$$

Moreover, the derivative matrices, J_c , J_k and J_m are obtained by differentiating the coefficient matrices C_n , K_n and M_n^+ with respect to the unknown vector $\boldsymbol{a}_n$, respectively. This is usually accomplished at the element level. The derivative matrices, J_c , J_k and J_m are detailed in Appendix VI as Eq.(VI.2).

The main steps in the computer code developed for solving Eq.(16) can be devised into two major steps, as shown in the flow charts, Figs.3.1 and 3.2. The integration of all necessary sub-matrices is conducted in the preparation stage, before starting the Newton-Raphson iteration. For example, the three integrals defined in Eq.(VI.1) are the three dimensional sub-matrices

$$K_{00} = \int_{\Omega_p} (\boldsymbol{\varphi} \bullet \boldsymbol{\varphi}^T) N_{xy} dA$$

$$B = \int_{d_1}^{d_2} (\boldsymbol{\psi} \bullet \boldsymbol{\psi}^T) N_z dz = \int_{-1}^{1} (\boldsymbol{\psi} \bullet \boldsymbol{\psi}^T) N_z d\xi \bullet \frac{(d_2 - d_1)}{2}$$

$$C = \int_{t_1}^{t_2} (\boldsymbol{\theta} \bullet \boldsymbol{\theta}^T) N_t dt = \int_{-1}^{1} (\boldsymbol{\theta} \bullet \frac{\partial \boldsymbol{\theta}^T}{\partial \tau}) N_t d\tau$$

which can be integrated independently from the solution procedure. On the other hand, the elemental matrices as indicated by Eq.(VI.2) are the results of tensor product which can be constructed only after the order of approximation and the new solution, a_n, are known. Thus, the formation of the elemental matrices as well as the matrix equation of Eq.(16) can only be done during the Newton-Raphson's iteration.

IV. Sensitivity Analysis

Since the matrix equation, Eq.(15), is in the form of a static problem, $A(x)x=c$. Differentiation of Eq.(15) with respect to a design variable, b, gives a sensitivity equation for a nonlinear transient heat transfer problem as,

$$(C + K + M^{+} + J_c + J_k + J_{M^{+}}).\frac{da_n}{db}$$

$$= -\left(\frac{dC}{db} + \frac{dK}{db} + \frac{dM^{+}}{db}\right)a_n + \frac{dM^{-}}{db}a_{n-1} + M^{-}\frac{da_{n-1}}{db} + \frac{dq}{db} \qquad (18)$$

The derivative matrices appearing on the right-hand side of Eq.(18) are not available yet in analysis phase, but needed for sensitivity analysis. Generation of such matrices can be tedious and prone to mistakes. A typical derivative matrix, dC/db, is given in Appendix VI. Fortunately, because of the nature of approximation, those derivative matrices can be obtained in the same way as the original matrices themselves. This becomes evident by comparing Eqs.(VI.1) and (VI.3) in Appendix VI. Furthermore, it is noted that Eq.(18) is a linear equation of $\frac{da_n}{db}$, which enjoys the same left-hand side coefficient matrices as Eq.(16). Thus, the factored matrices saved from analysis at the converged stage, can be reused here to solve the sensitivity equation. That makes the sensitivity analysis computationally efficient.

V. Numerical Results

The numerical experiences on development and application of the p-version Galerkin's method are reported here in three separated sections. One main focus here is studying the accuracy of the proposed method for analyzing an example, nonlinear, transient heat conduction problem. The sources of errors may come from the approximation in the temperature interpolation, in the nonlinear material relation and in the thermal loads, boundary and initial conditions. Section IV.1 investigates the errors due to approximation in temperature and in nonlinearity. Section IV.2 studies the heat conduction under a moving point heat source. The heat source is represented by a singular delta function. It is expected that the error is resulted from lacking of regularity in loading. However, the results summarized in Section IV.2 represent only an initial attempt on the subject. Further study is needed in this regard. Section IV.3 shows the results of sensitivity analysis which demonstrate possible use of sensitivity values.

V. 1. Study of Accuracy

Two examples, one is in 2D and the other in 3D, are used to study four aspects of accuracy by varying the orders of approximation in time, space and material nonlinearity, by increasing the time and by reducing the size of elements. The 2D problem is a 1x1 square with the exact solution being given as

$$u_e(x,y,t) = xy(x-1)(y-1)t^5 \tag{19}$$

,whereas the 3D problem is a 1x1x1 block with the exact solution being given as

$$u_e(x,y,t) = xy(x-1)(y-1)(2\psi_2(z)+3\psi_3(z)+4\psi_4(z)+5\psi_5(z))t^5 \tag{20}$$

where $\psi_i(z)$ is an integrated Legendre polynomial of order i, as described in Appendix III. The solutions in both cases satisfy the homogeneous boundary conditions and zero initial condition. And the material properties, ρc and isotropic k, used in these cases are assigned by a linear temperature relation,

$$\rho c, k = \alpha + \beta u \tag{21}$$

where α and β are assigned constants.

It should be noted that to achieve the exact solutions as described by Eqs.(19-20), the orders of the in-plane temperature, the through-thickness and the time approximation, denoted by P_{xy} , P_z, and P_{time}, should be at least 4, 5 and 5, respectively. Since material properties are linearly related to the temperature as given by Eq.(21), the orders of the in-plane, the through-thickness and the time approximation, denoted by M_{xy}, M_z and M_{time}, should be at least 4, 5 and 5, respectively, as well. The results reported here focus on the accuracy of the solutions which are subjected to varied orders of such approximation.

Reduction of Errors due to Increase of Order of Approximation in Time

For linear transient heat conduction problems with smooth solutions, the L^2-norm of the error is bounded by

$$\|e\|_{L^2(\Omega\times I)} \le C\Delta t^{(P_{time}+1)} \tag{22}$$

where the pointwise error, $e = u - u_e$, and u and u_e denote the numerical and the exact solutions, respectively. The L^2-norm error is defined for a 2D case as

$$\|e(t)\|_{L^2} = \left\{ \int_0^T \left[\int_\Omega \left[\left(\frac{\partial e}{\partial x} \right)^2 + \left(\frac{\partial e}{\partial y} \right)^2 + e^2 \right] dxdy \right] dt \right\}^{1/2} \tag{23}$$

The corresponding 3D case can be defined in a similar manner.

The log-log plot of Fig.5.1.1 for the 2D linear transient problem shows that the L^2-norm of error is linearly proportional to the order of approximation in time, (P_{time}+1), as indicated by Eq.(22). In addition, the results of the 2D nonlinear transient problem shown in Fig.5.1.2 show an identical, linear relation. Similar trends are also observed in the 3D linear and nonlinear cases as shown in Figs. 5.1.3 and 5.1.4. Note that in the nonlinear cases studied here, β=10 in Fig.5.1.2 and β=1 in Fig. 5.1.4. Furthermore, the order of approximation in time for material distribution is maintained at 5 for both nonlinear cases.

To investigate the change of errors along with time, the pointwise error, $H^1(\Omega)$, of time, defined below for a 2D case, is used hereafter,

$$\|e(t)\|_{H^1(\Omega)} = \left\{ \int_\Omega \left[\left(\frac{\partial e}{\partial x} \right)^2 + \left(\frac{\partial e}{\partial y} \right)^2 + e^2 \right] dxdy \right\}^{1/2} \tag{24}$$

The results of the linear case are summarized in Figs. 5.1.5. Figure 5.1.5(a) shows the increase of errors for a longer simulation time period. The effects of orders of approximation in time on the error distribution within a single time interval are detailed in Figs.5.1.5(b) and (c). Similar trend can be observed in the 3D case as shown in Figs. 5.1.6. It is noted from Figs.5.1.5(a) and 5.1.6(a) that the nonlinear case has a bigger jump of temperature discontinuity crossing the interfaces of time intervals than the linear case does.

Reduction of Errors due to Reduction of Element Sizes

For linear transient heat conduction problems with smooth solutions, the H^1-norm of the error is bounded by

$$\|e(t)\|_{H^1(\Omega)} \le C h^{\min(P_{xy}, P_z)} \tag{25}$$

The results of two analyses with different meshes are summarized in Fig.5.1.7 for both linear and nonlinear cases, where the square-root of element area, $\sqrt{Area}$, is used to represent the element size, h. The analysis domain is meshed into 4-element and 16-element cases, as shown in Fig.5.1.8. Another parameter studied here is the orders of polynomials for in-plane approximation of temperature as denoted by P_{xy} for the nonlinear case and LP_{xy} for the linear case in Fig.5.1.7. The results show that Eq. (25) is closely observed for the cases when the orders of polynomials are 2 and 3 for both linear and nonlinear cases. Note that the correct solution is achieved, if the order of polynomials reaches 4.

Increase of Errors due to Increase of Nonlinearity

Two 3D, nonlinear transient problems are solved with β=1 and β=4 which represent different degrees of nonlinearity in material-temperature relation defined in Eq.(21). Figure 5.1.9 shows that the degree of nonlinearity can aggravate the error caused by inadequate approximation. In this study, the only parameter varied is the order of polynomials used in time domain approximation.

Increase of Error due to Increase of Simulation Time Period

In this study, the time step is set to be 1 second and the total operational time, τ, is set to be 4 seconds. The orders of in-plane and the temporal polynomials are selected to be 4 and 6, respectively, for temperature interpolation as described by Eq.(11), whereas the orders of in-plane and the temporal polynomials are 3 and 5, respectively, for material property interpolation, Eq.(12). The total Lagrange points for the in-plane material interpolation is 10 as marked in Fig.5.1.10. Moreover, the error is measured by the L^2-norm as defined by Eq.(23).

At the end of the first time interval, $t_1 = 1$ second, the error is in the order of 10^{-4}. The error is growing with the time. At $t_2 = 2$ second, the error grows to the order of 10^{-1}. At $t_4 = 4$, the error becomes 13.31. The major source of the error is expected to be the deficiency in the in-plane interpolation of materials. Since the material property is linear in temperature, it's exact order of interpolation has to be 4, equal to the order of temperature interpolation. However, in this study, the order used is 3. Such kind of error can be aggravated from one time interval to the next. The results of the exact temperature distribution are shown in Fig. 5.1.11.

V. 2. Heat Transfer Analysis with a Moving Heat Source

An attempt is made here to simulate the welding process in which the testing article is subjected to a moving point heat source. Let the point heat source move along with y-axis with constant velocity, v, and an intensity, q. Thus, the point heat source is represented as

$$Q = q \times \delta(x - \bar{x}, y - \bar{y}) \tag{26}$$

where in our study, $\bar{x}$ is fixed and $\bar{y}$=tv. The equivalent heat source vector can be obtained by the following equation,

$$\begin{aligned} \boldsymbol{q} &= \int_{I_n \Omega_e} \int q \times \delta(x - \bar{x}, y - \bar{y}) \chi dA dt \\ &= \int_{I_n \Omega_e} \int q \times \delta(x - \bar{x}, y - \bar{y}) \left[\varphi(x, y) \otimes \theta(t)\right] dA dt \\ &= \int_{I_n} q \times \left[\varphi(\bar{x}, \bar{y}) \otimes \theta(t)\right] dt \end{aligned} \tag{27}$$

The area coordinates corresponding to $\bar{x}$ and $\bar{y}$ can be found in a triangular element defined by three vertices, (x_i, y_i), i=1 to 3, as

$$\bar{x} = L_1 x_1 + L_2 x_2 + L_3 x_3$$
$$\bar{y} = tv = L_1 y_1 + L_2 y_2 + L_3 y_3$$
$$1 = L_1 + L_2 + L_3$$

with which $\varphi(\bar{x}, \bar{y})$ can be expressed in terms of t explicitly. Equation 27 can then be integrated to obtain the equivalent thermal load vector in a given time interval.

Two meshes are studied here; 4-element and 48-element models as shown in Fig.5.2.1. The temperature distributions resulted from linear simulation are shown in Figs.5.2.2 and 5.2.3 at time instances equal to 0.1 second and 1 second, respectively, based upon a 4-element mesh. The advance of the high temperature zone is evident from these two figures. However, the movement of the highest temperature spot is about 4 time faster than that of the point heat source. Furthermore, the highest temperature obtained from a 48-element mesh, as shown in Fig.5.2.4, is about 40 percent higher than that obtained from a 4-element mesh. These observations make the simulated results unacceptable. It is expected that the singularity of the point load given by Eq.(26) causes numerical difficulty. Further study is needed to gain better understanding of such type of application of the p-version Galerkin's method.

V. 3. Sensitivity Analysis

The material properties studied here are considered temperature-dependent. Therefore, any parameters that define the material-temperature relation can be considered as a design variable. In Case 1, the slope of such relation is considered as a design variable. Furthermore, since the temperature is modeled as a distributed function within an element, the material properties here can also be viewed as distributive. Therefore, the material distribution within an element can be viewed as a design variable as well, regardless whether the problem is nonlinear or not. In Case 2, the material properties – the thermal conductivities at the Lagrange points of the entire problem are considered as design variables. In order words, it is the material distribution considered as a design variable in Case 2.

Case 1

The slope of the thermal conductivity-temperature relation is considered as a design variable. Since only the matrix K depends upon this special design variable, the right-hand side of Eq.(18) can be greatly reduced to a single term, $(dK/db)\boldsymbol{a}$. The results of the thermal sensitivity coefficients at times from 1 second to 4 seconds are shown in Fig.5.3.1. Note that the thermal sensitivity coefficients is interpolated in the same way as the temperature; i.e.,

$$\frac{du}{db} = \chi^T(x,t)\frac{d\boldsymbol{a}}{db}$$

where da / db is obtained from Eq.(18). Comparing with the finite differencing, the errors of the thermal sensitivity coefficients are less than 10^{-4} for all the time intervals.

Case 2

Since in this study, the material property is assumed to be a distributed function, one may then assume that the square slab is made of various materials. In this particular case, the value of k at each Lagrange point is determined by it's own material table. If the slope of each material table is considered as a design variable, there are 10 independent design variables in total, as marked in Fig.5.1.10.

Figures 5.3.2 and 5.3.3 show the distributions of the thermal sensitivity coefficients of du / db_1 and du / db_9, where b_1 and b_9 are the slopes of the thermal conductivity-temperature relations at Lagrange points 1 and 9, respectively. The figures reveal that the design variable, b_1, affects the change of temperature along the diagonal line, whereas the design variable, b_9, does the same to the area off the diagonal line more. Finally, all 10 thermal sensitivity coefficients of the temperature at the center point are collected and plotted out in Fig.5.3.4. The picture indicates the degree of influence of individual design variable on the temperature at the center location at different time instances; i.e., $\partial u(x_c, y_c) / \partial b_i, i = 1$ to 10. It is as expected that the figure shows that the value of the thermal conductivity at the center affects the temperature at the same point the most.

VI. Discussions and Remarks

The report documents the effort in the development of a structural-compatible code for nonlinear heat transfer analysis and sensitivity analysis based upon the framework of the p-version time-discontinuous Galerkin's method. Numerical studies are made to assess the performance of the method.

It is found that the error characteristics of the method in solving the nonlinear problem are very similar to that of the linear one, if the degree of nonlinearity is small. The high degree of material nonlinearity can aggravate the numerical errors through the approximation in material distribution. Furthermore, a better approach is needed to convert general, pointwise descriptions of the loading, boundary and initial conditions into equivalent and consistent vector forms. These concerns point to the need of developing an adaptive method for error control. Note that the leading elemental matrix in the transient problem is non-singular. This observation makes the element-by-element error correction scheme[5] developed for linear, static problems very attractive to the nonlinear, transient problems studied here.

An attempt is also made to find the thermal sensitivity based upon the p-version time-discontinuous Galerkin's method. The parameters that are related to the material-temperature dependent relation as well as the material distribution are

considered as design variables in this study. Though construction of the matrix equation for thermal analysis is complicated, construction of that for thermal sensitivity analysis is rather simple. Solving the resultant sensitivity equation is also demonstrated to be computationally efficient.

Although the *p*-version Galerkin's method can effectively achieve an order of reduction in meshing effort, the size of the matrix equations remains large for solving a 3D problem. An effective iterative solution strategy for a non-symmetric matrix equation is needed in order to support more challenging applications of the proposed method.

References

1. Tomey, J. P., "The *p*-Version Discontinuous Galerkin Method for Heat Transfer in Built-up Structures," M.S. Thesis, George Washington University, May, 2001.
2. Walker, D. T., "Nonlinear Conduction Heat Transfer Using a Hierarchical Finite Element Method," M.S. Thesis, George Washington University, June, 2003.
3. Kaneko, H.. and Bey, K. S., "Error Analysis of *p*-Version Discontinuous Galerkin Method for Heat Transfer in Built-up Structures," (in preparation)
4. Szabo, B., Babuska, I., *Finite Element Analysis*, John Wiley & Sons, New York, 1991.
5. Lang, C. G., "Finite Element *A Posteriori* Error Estimation for Heat Conduction," M.S. Thesis, George Washington University, June, 2000.

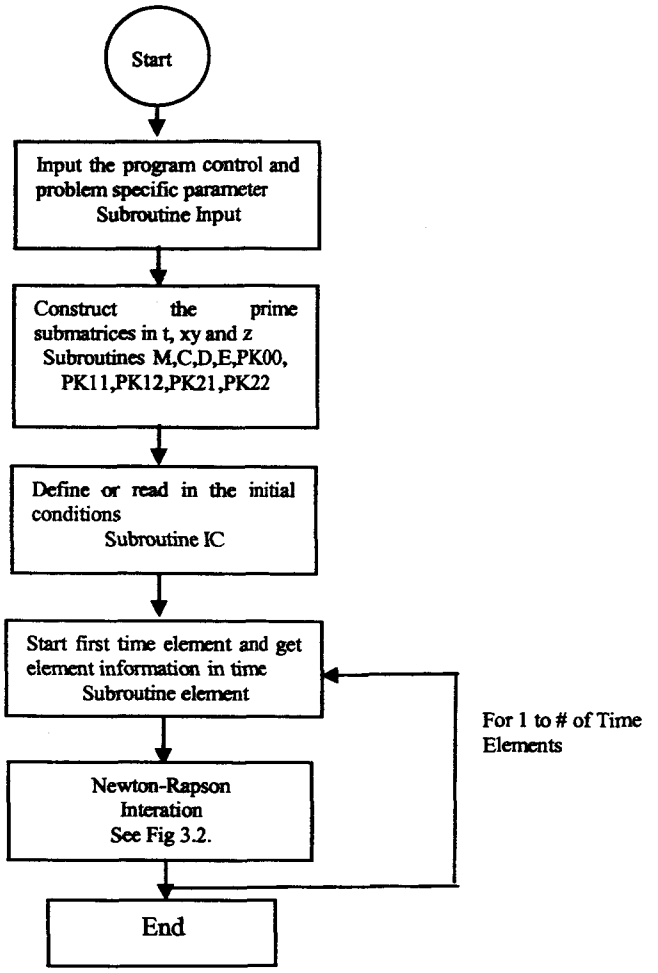

Figure 3.1. The Prepration Stage and Marching through Time Intervals

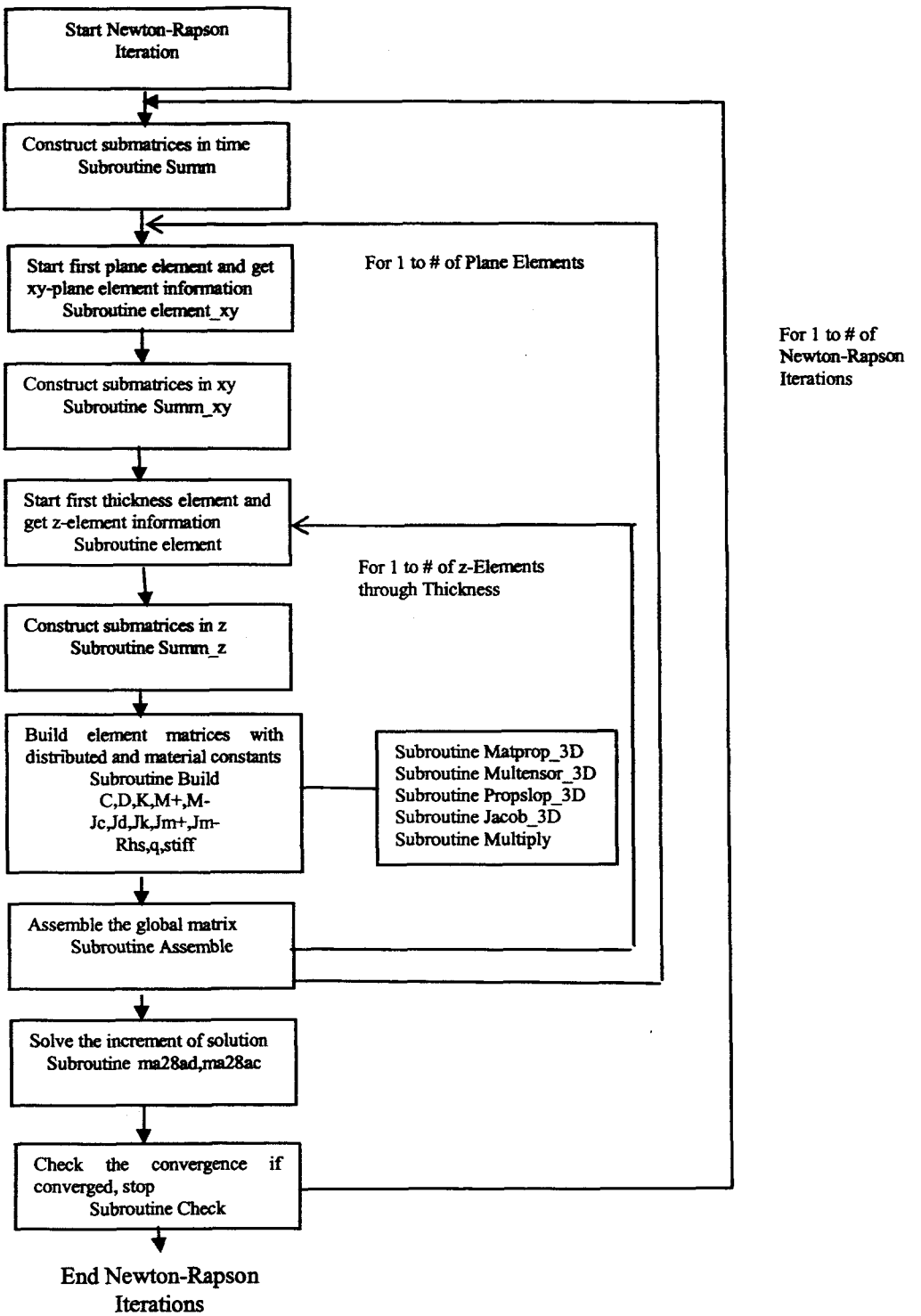

Figure 3.2. The Newton-Rapson Iteration for a Single Time Interval

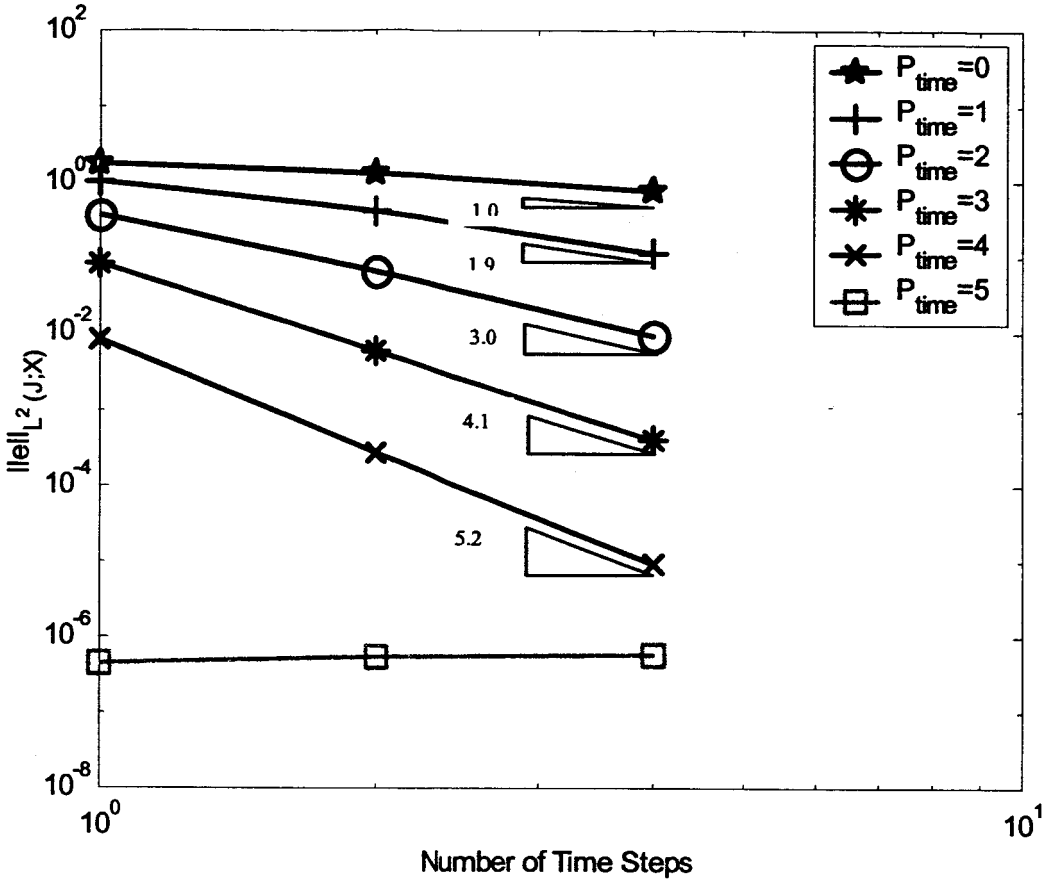

Figure 5.1.1. Error, $\|e\|_{L^2}$, versus Number of Time Steps;
2D, Linear Case, $P_{xy} = 4$ at $t = 2$ seconds

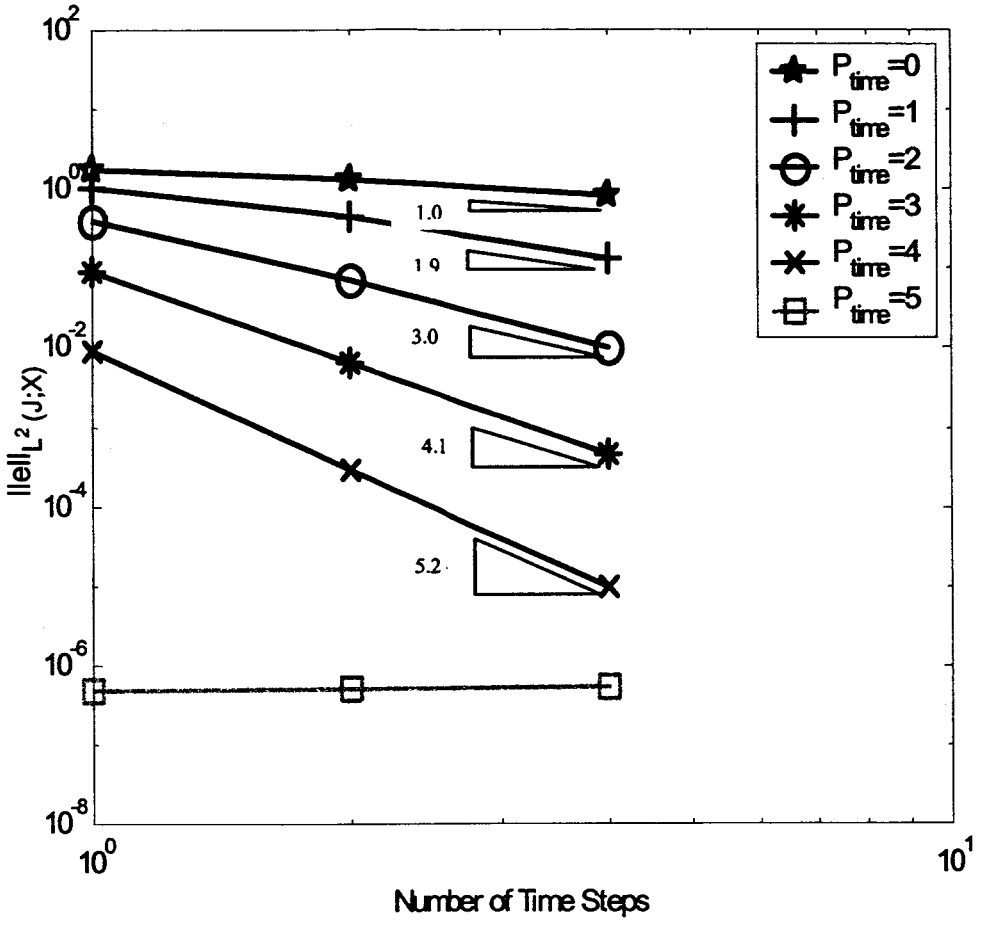

Figure 5.1.2. Error, $\|e\|_{L^2}$, versus Number of Time Steps;
2D, Nonlinear Case, $P_{xy} = M_{xy} = 4$ and $\beta = 10$ at $t = 2$ seconds

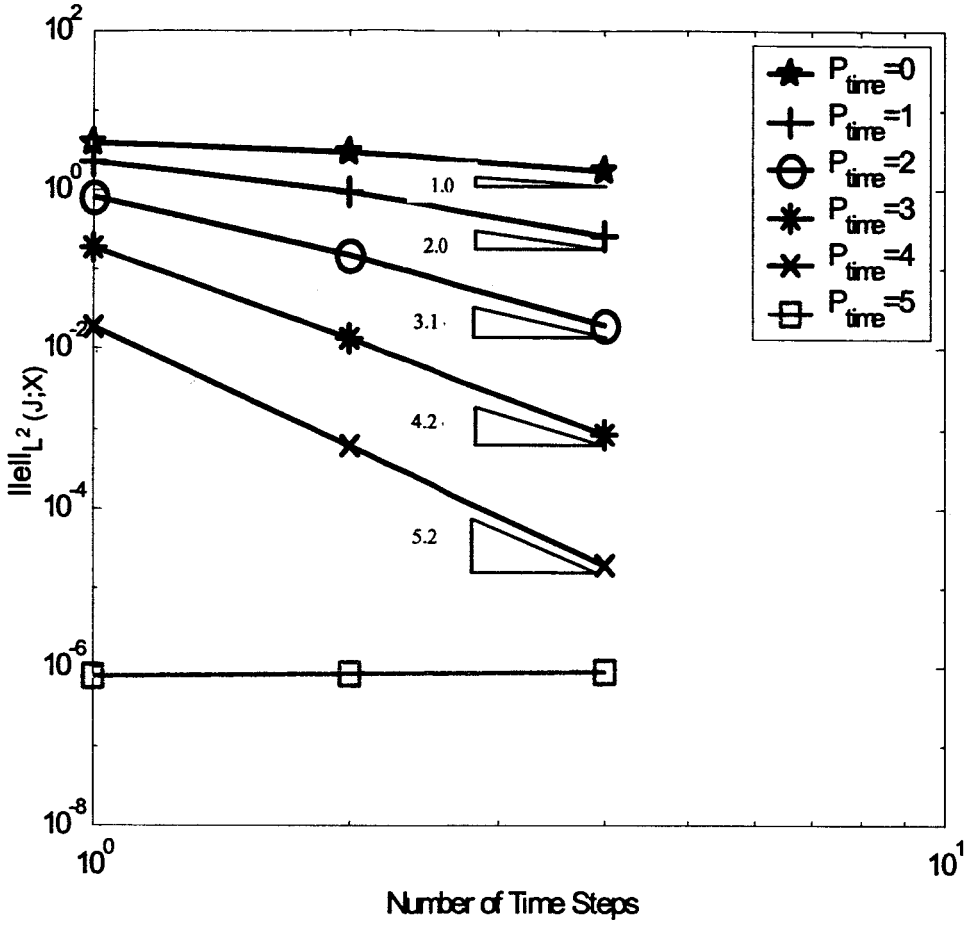

Figure 5.1.3. Error $\|e\|_{L^2}$ versus Time; 3D, Linear Case,
$P_{xy} = 4$, $P_z = 6$, at $t = 2$ seconds

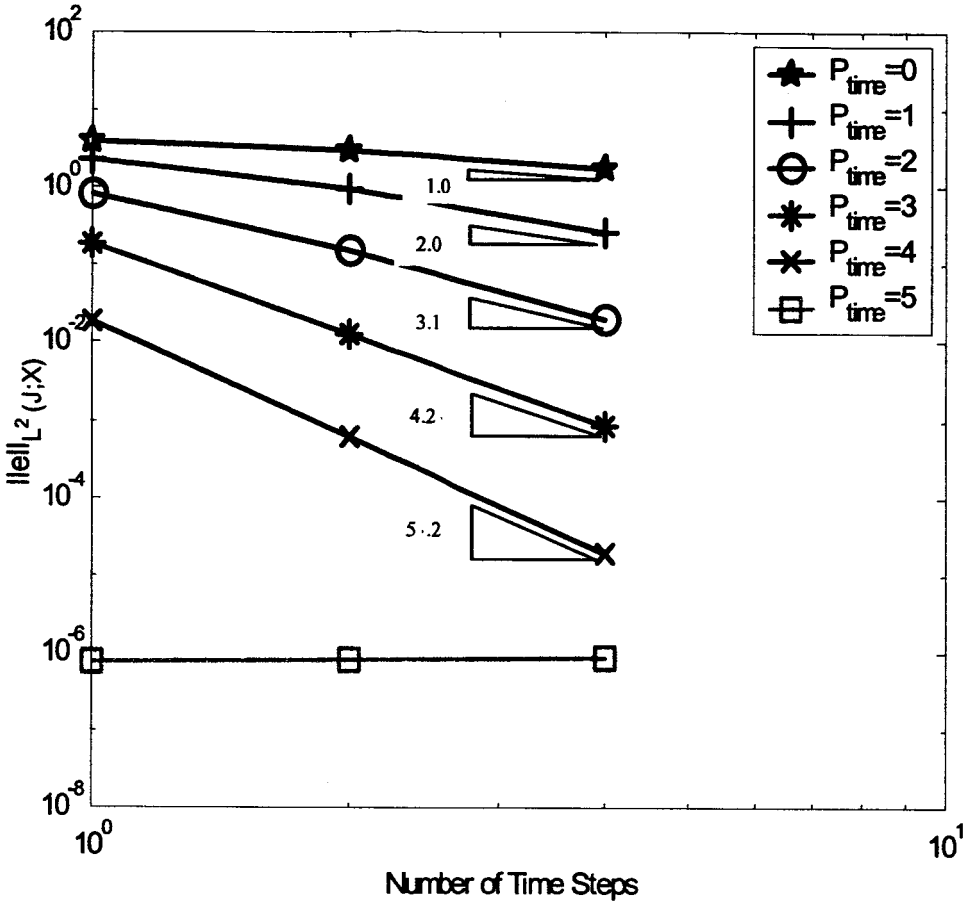

Figure 5.1.4. Error $\|e\|_{L^2}$ versus Time; 3D, Nonlinear Case,
$P_{xy} = M_{xy} = 4$, $P_z = 6$, $M_z = 5$ at $t = 2$ seconds

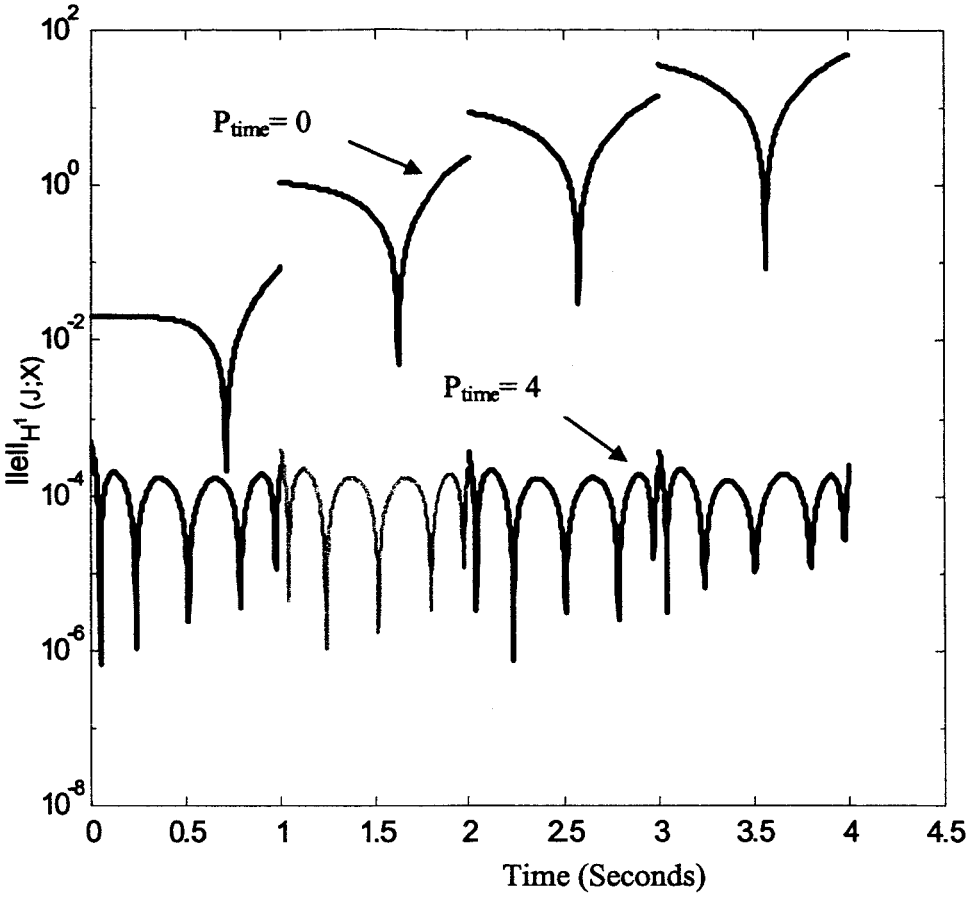

Figure 5.1.5(a). Global Error $\|e\|_{H^1}$ versus Time;
2D, Linear Case, $P_{xy} = 4, \Delta t = 1$ second

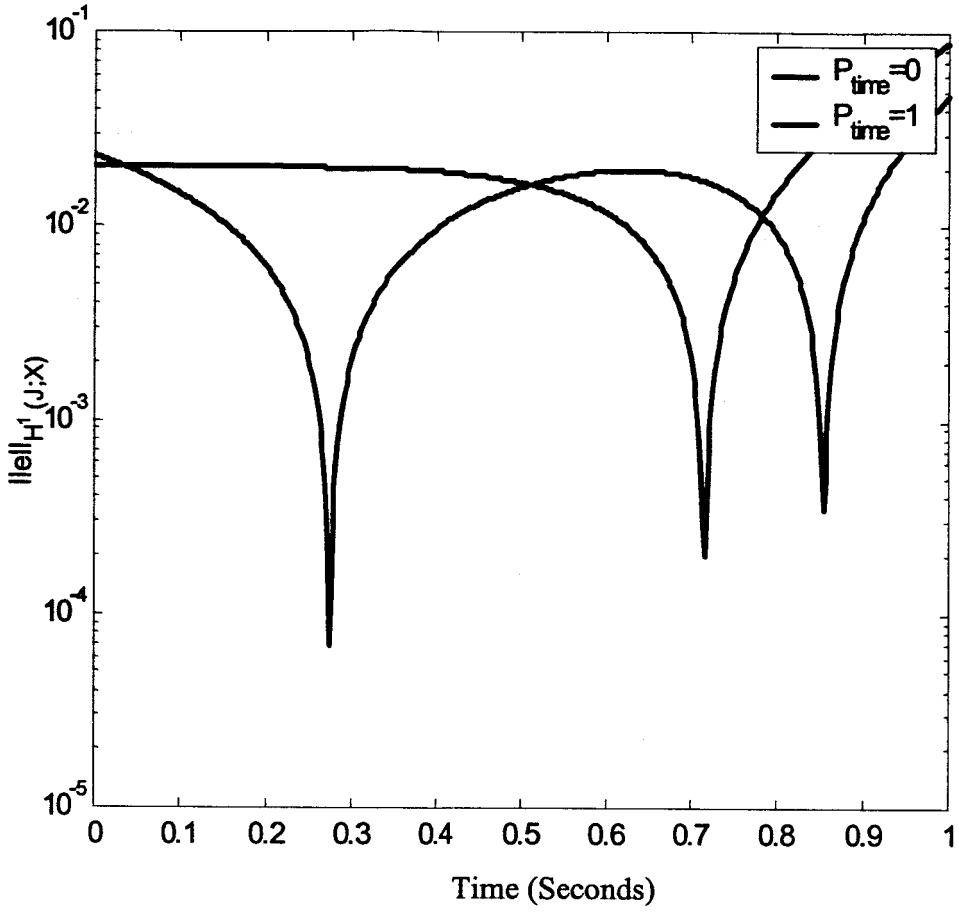

Figure 5.1.5 (b). Global Error, $\|e\|_{H^1}$ versus Time in One Time Interval for Linear Case; $P_{time} = 0$ and 1

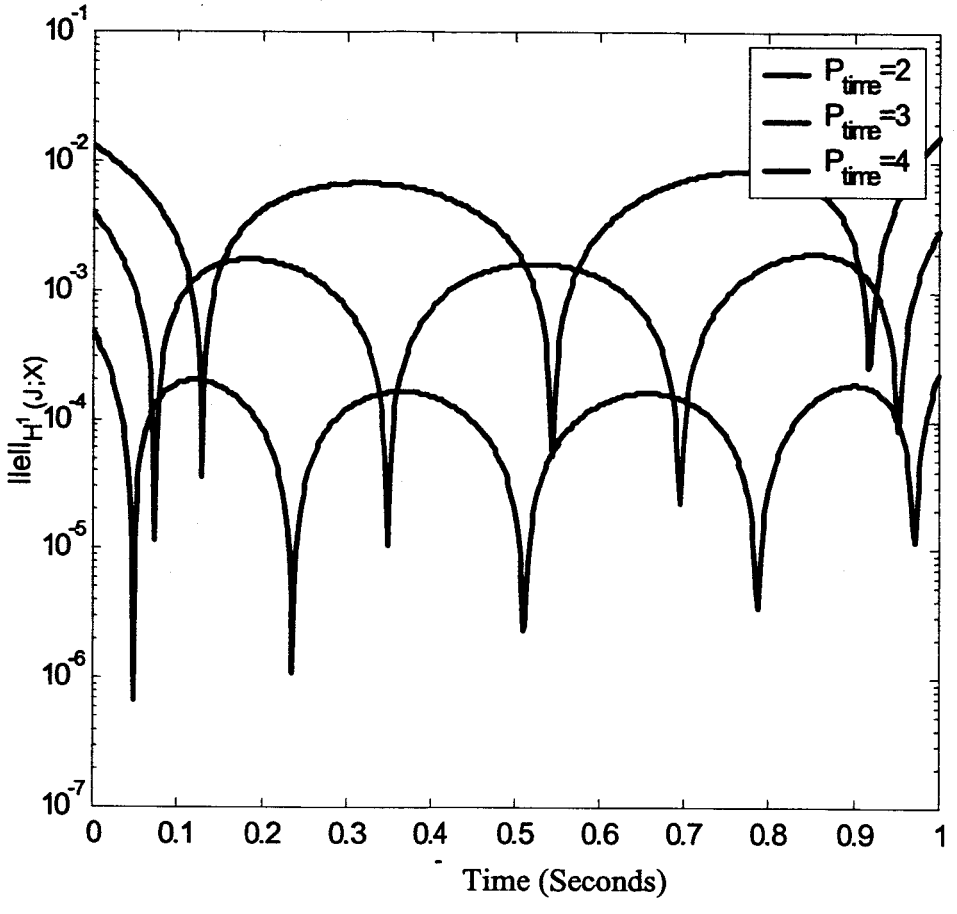

Figure 5.1.5 (c). Global Error, $\|e\|_{H^1}$ versus Time in One Time Interval for Linear Case; $P_{time} = 2, 3$ and 4

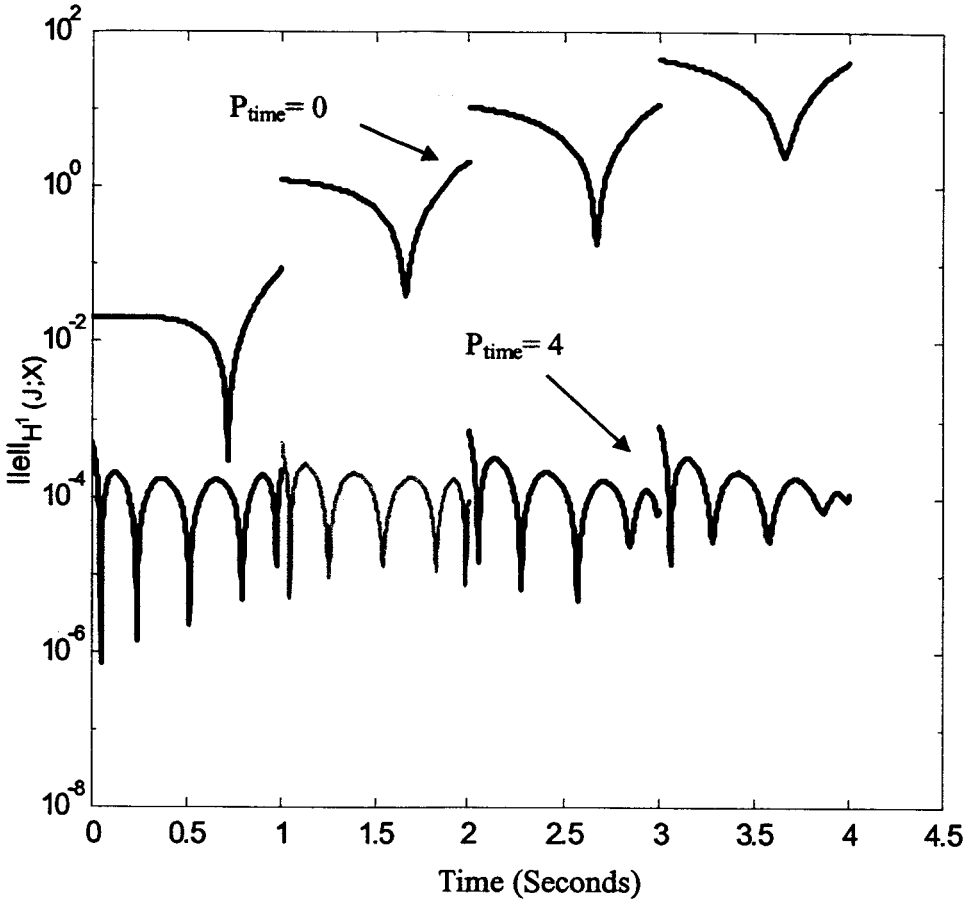

Figure 5.1.6(a). Global Error $\|e\|_{H^1}$ versus Time; 2D, Nonlinear Case, $P_{xy} = M_{xy} = 4, \Delta t = 1$ second

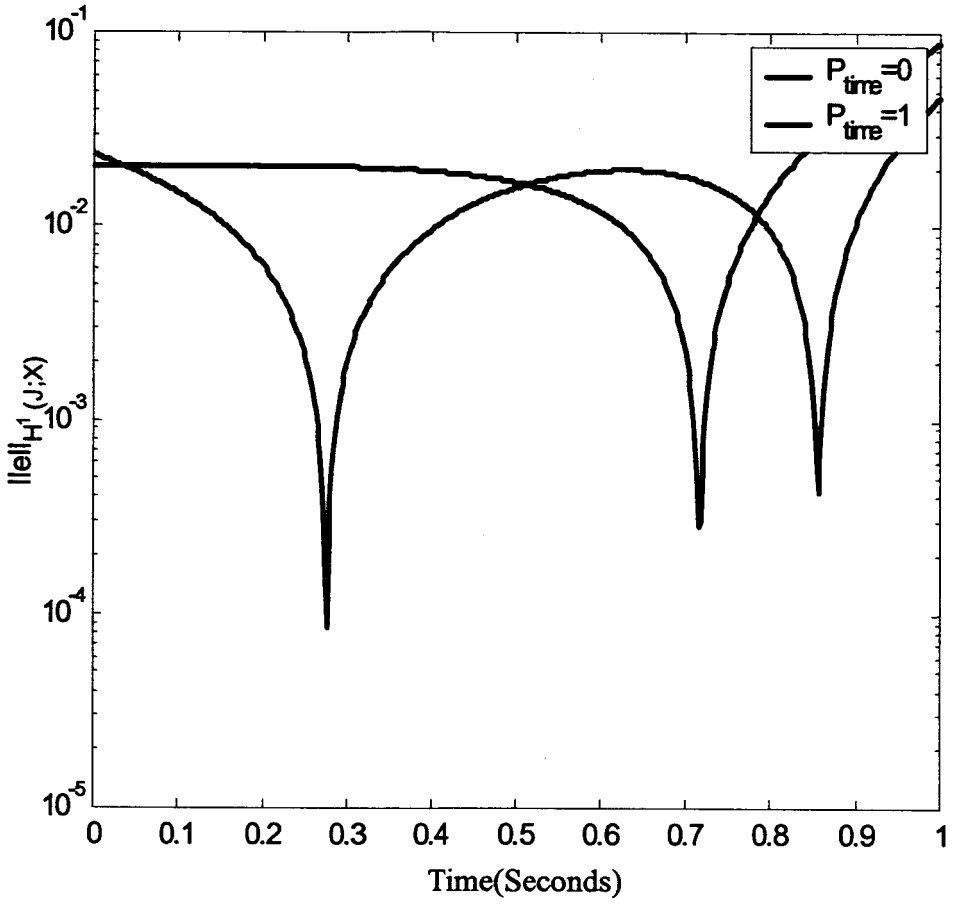

Figure 5.1.6(b). Global Error, $\|e\|_{H^1}$ versus Time in One Time Interval for Nonlinear Case; $P_{time} = 0$ and 1

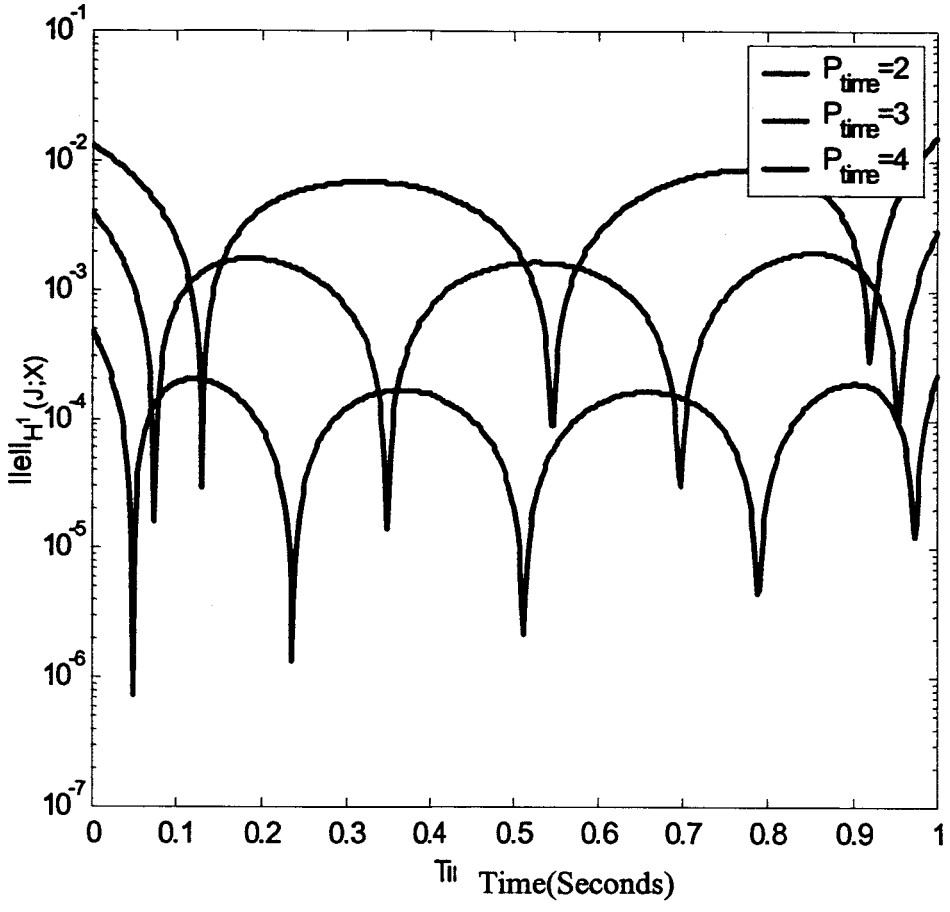

Figure 5.1.6(c). Global Error, $\|e\|_{H^1}$ versus Time in One Time Interval for Nonlinear Case; $P_{time} = 2, 3$ and 4

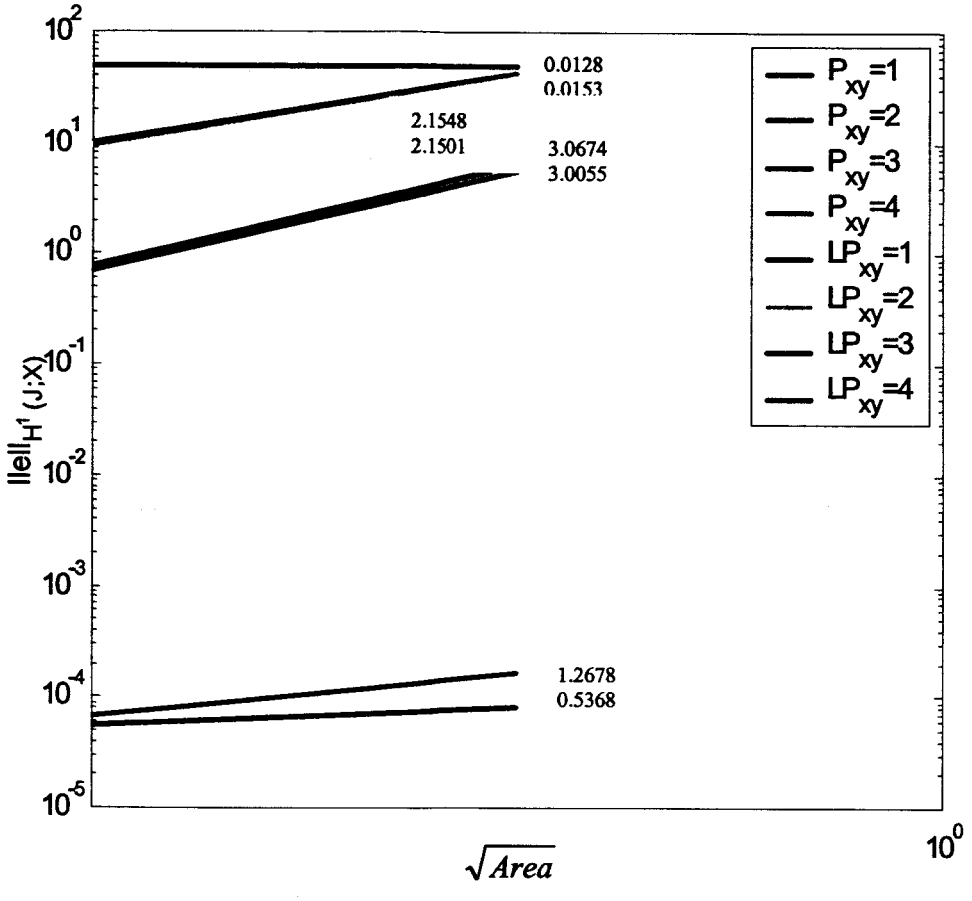

Figure 5.1.7. Effect of Element Size on Error at t = 2 seconds

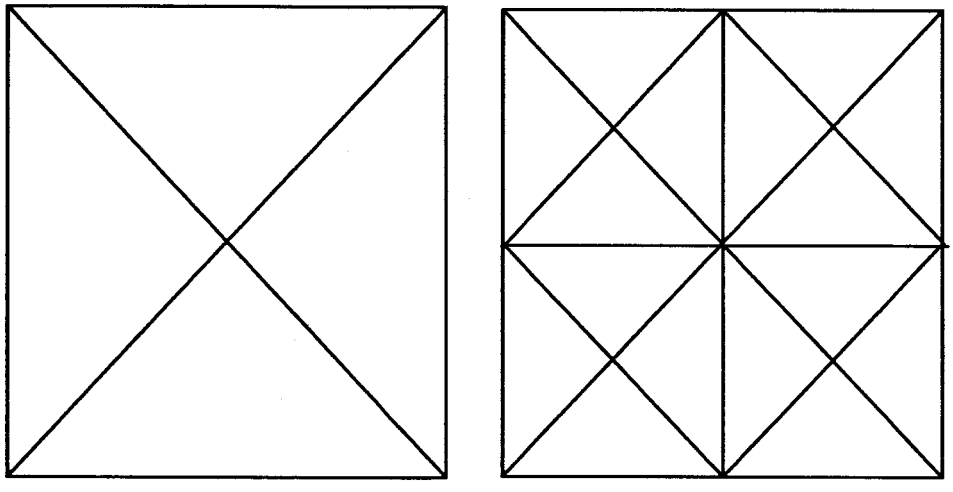

(a) (b)

Figure 5.1.8. (a) 4 Element Meshes
(b) 16 Element Meshes

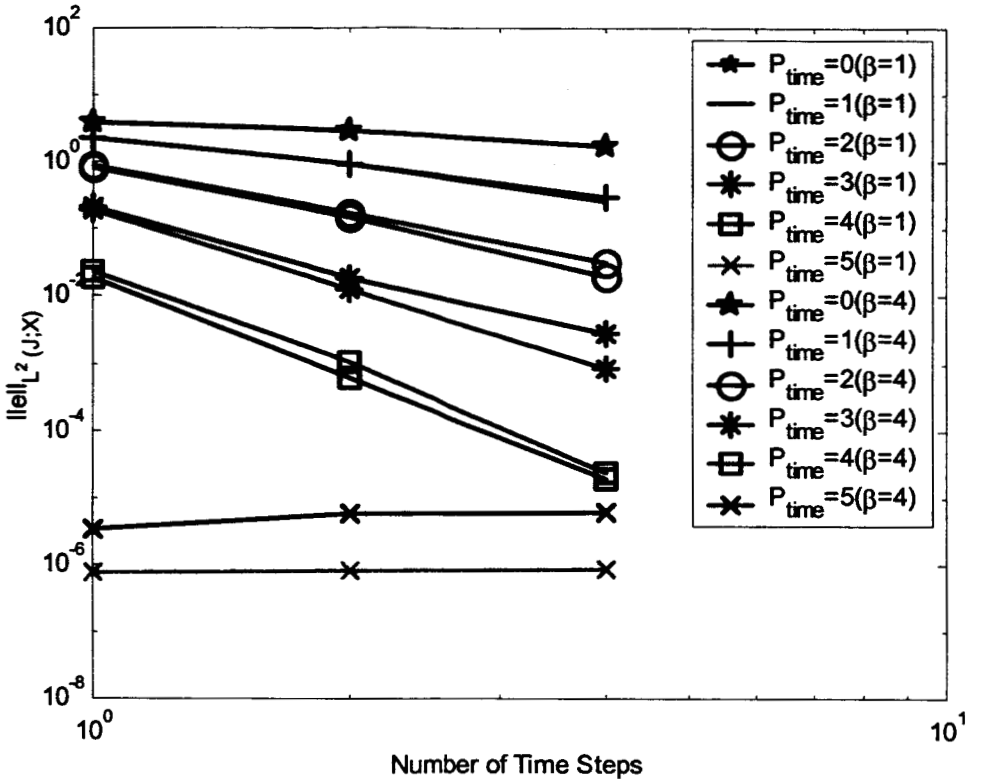

Figure 5.1.9. Errors due to Nonlinearity in Material-Temperature Relation at t=2 seconds (Convergence is very similar to Linear Case when $\beta = 1$)

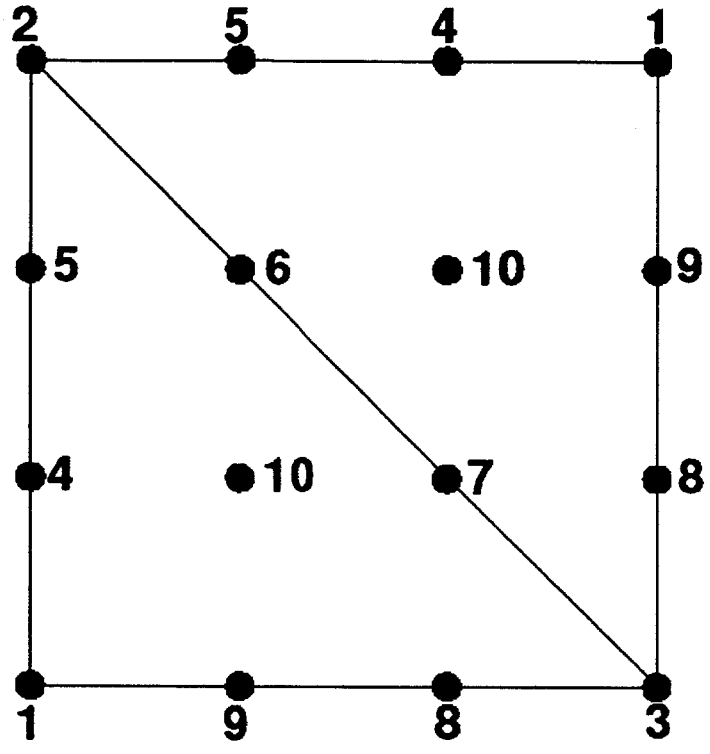

Figure 5.1.10. Meshes and Lagrange Points for Interpolation of Material Properties

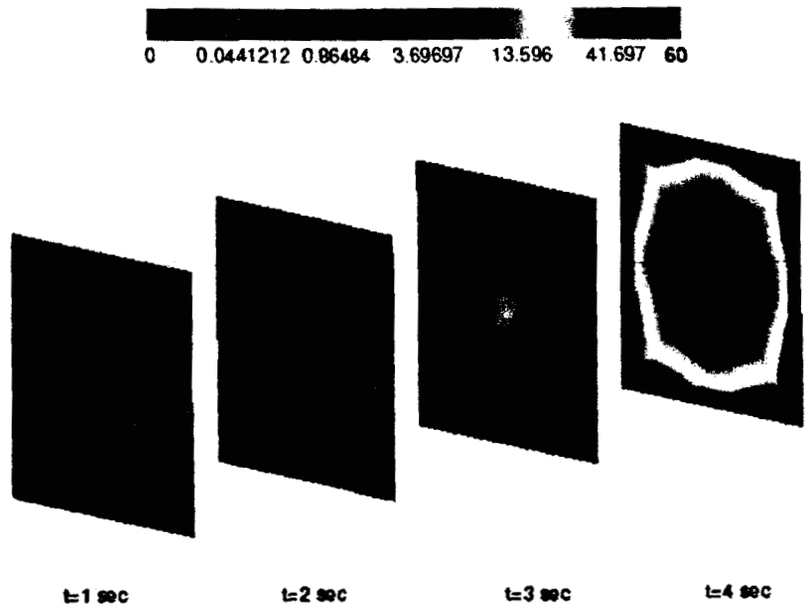

Figure 5.1.11.Exact Temperature Distribution

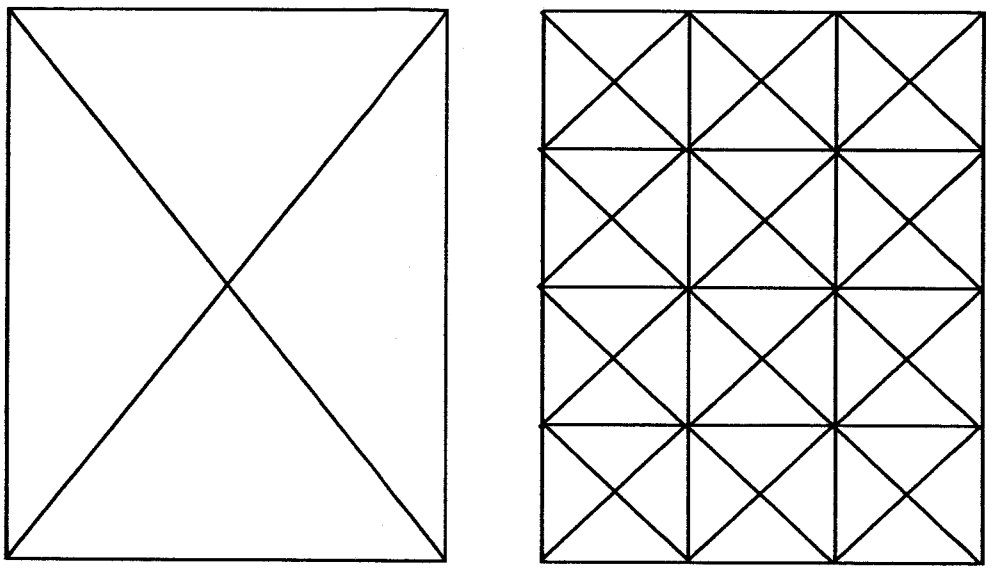

(a) (b)

Figure 5.2.1. (a) Meshes for 4 Element Model
(b) Meshes for 48 Element Model

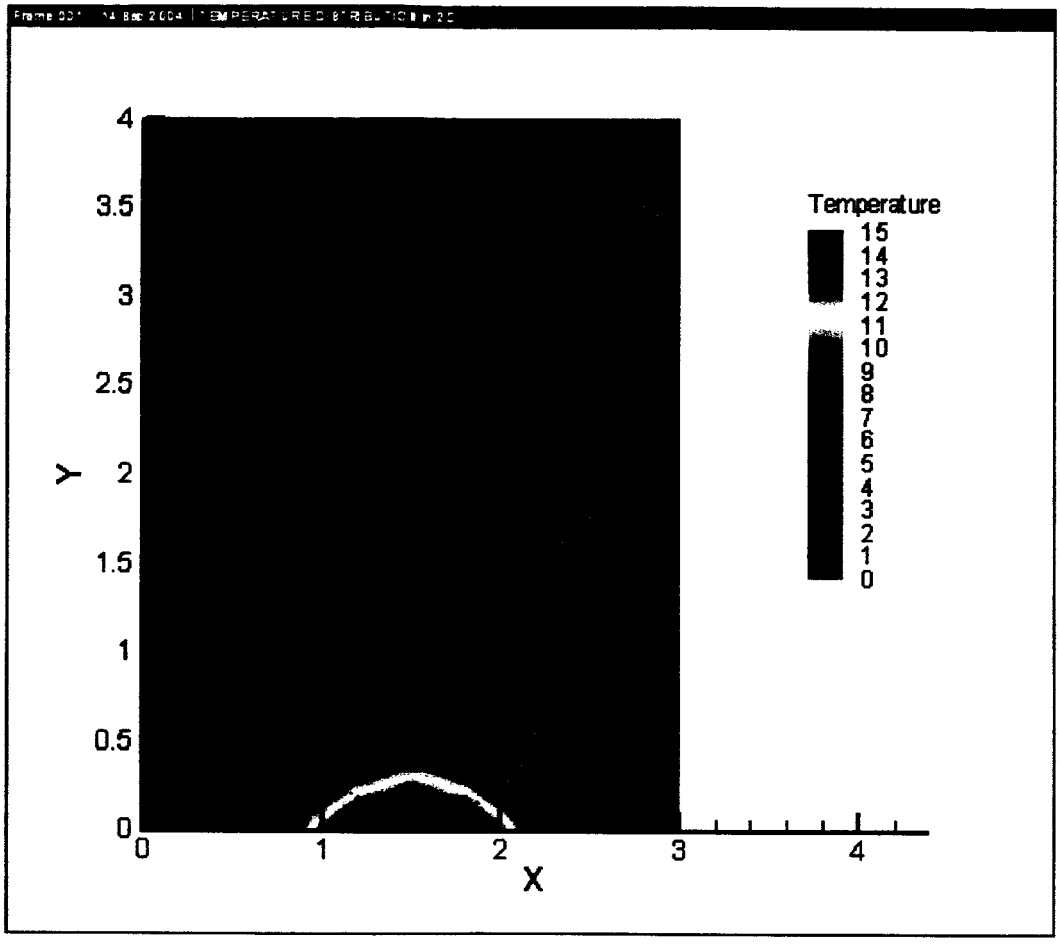

Figure 5.2.2. Temperature Distribution at t=0.1 Second for a 4-Element Model

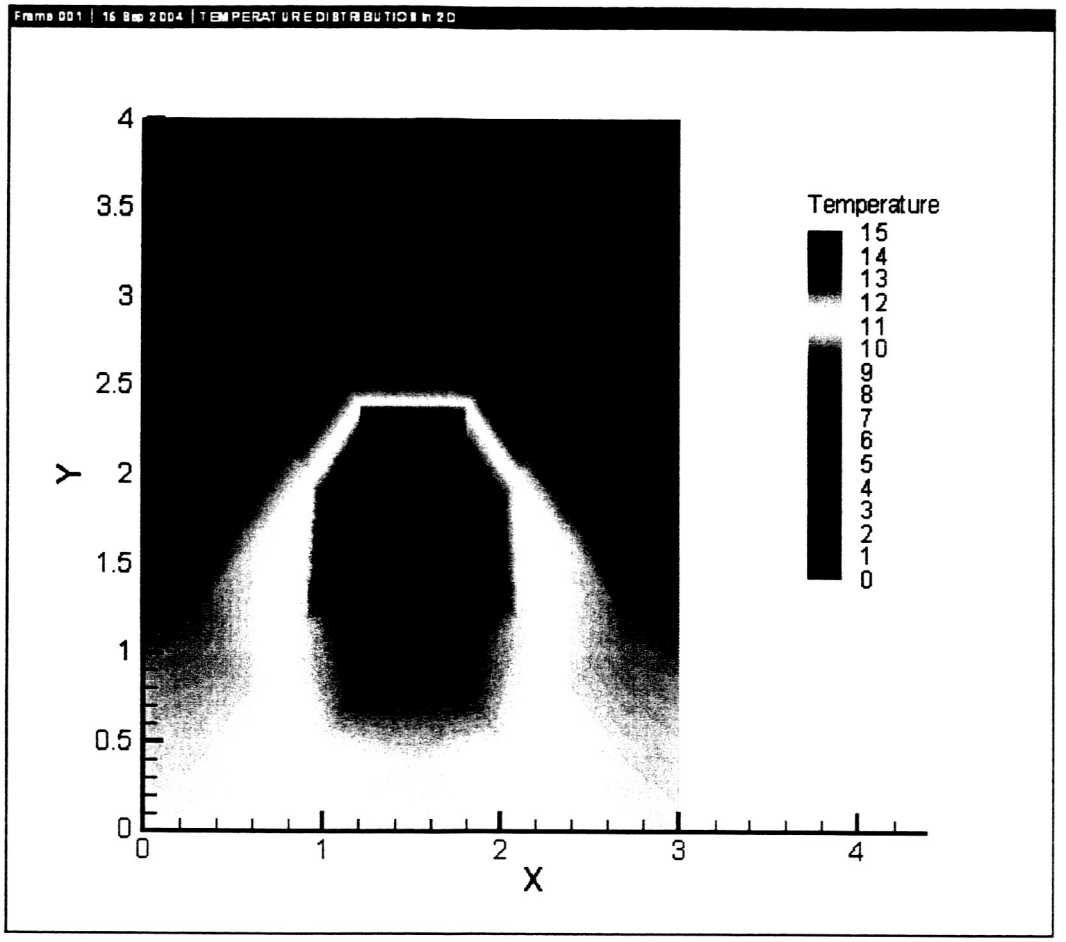

Figure 5.2.3. Temperature Distribution at t=1 Second for a 4-Element Model

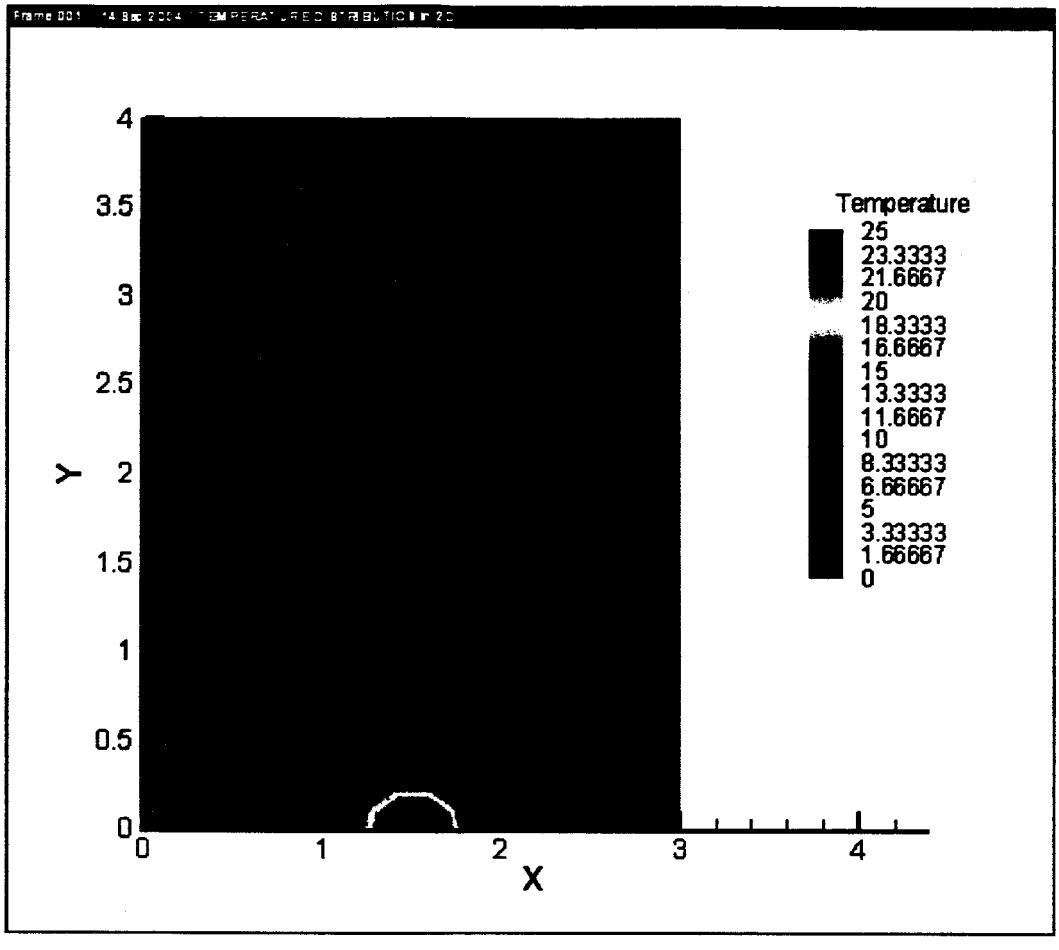

Figure 5.2.4. Temperature Distribution at t=0.1 Second for a 48-Element Model

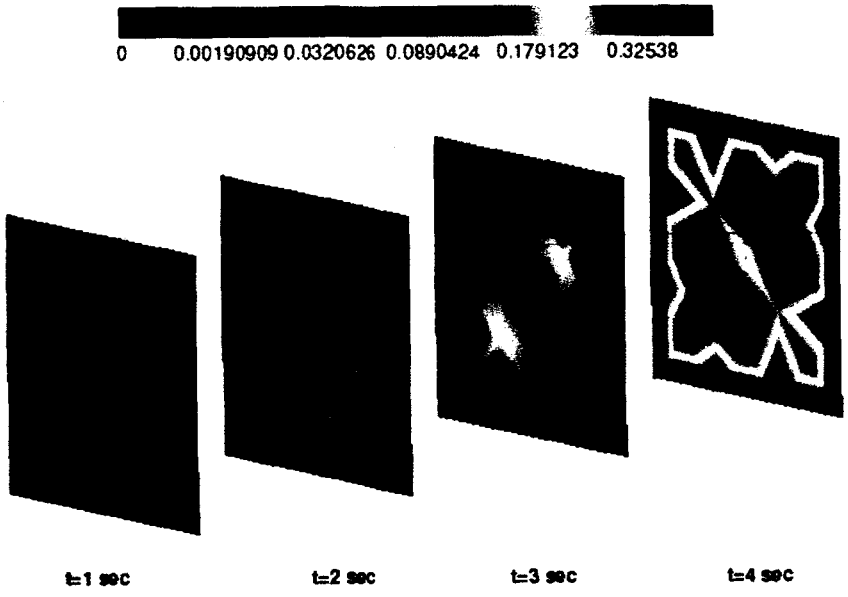

Figure 5.3.1. Coefficients of Thermal Sensitivity with Respect to Homogeneous Thermal Conductivity; $\frac{\partial u(x,y)}{\partial b}$.

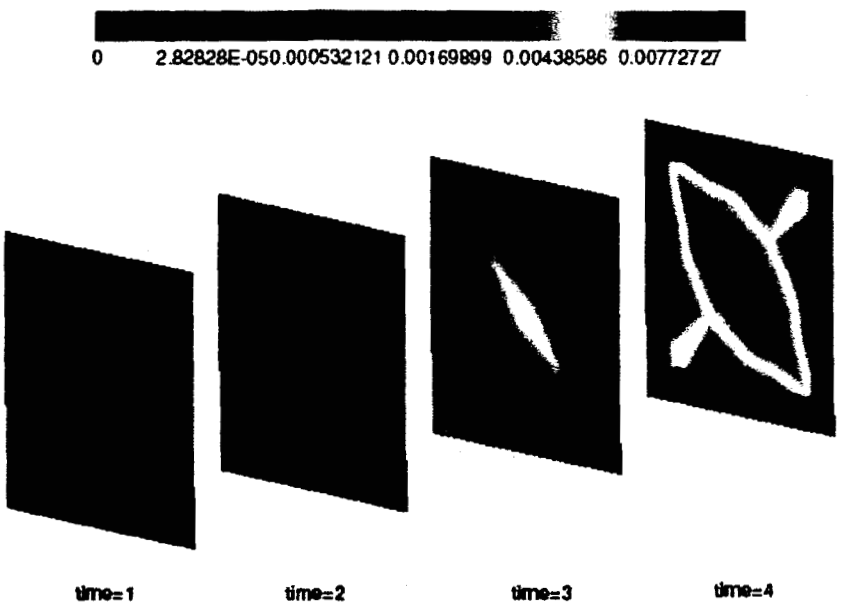

Figure 5.3.2. Coefficients of Thermal Design Sensitivity with Respect to Thermal Conductivity at Material Lagrange Point 1; $\frac{\partial u(x,y)}{\partial b_1}$.

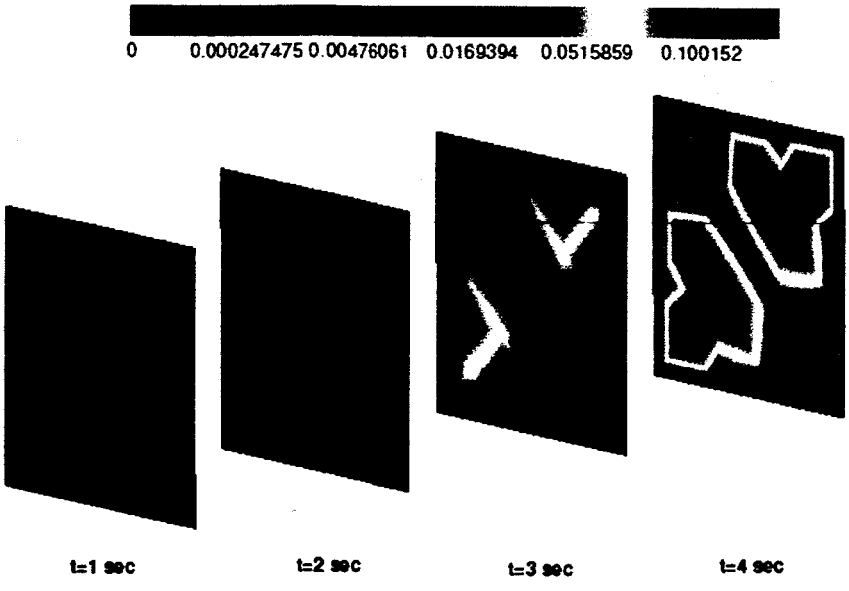

Figure 5.3.3. Coefficients of Thermal Design Sensitivity with Respect to Thermal Conductivity at Material Lagrange Point 9; $\frac{\partial u(x,y)}{\partial b_9}$.

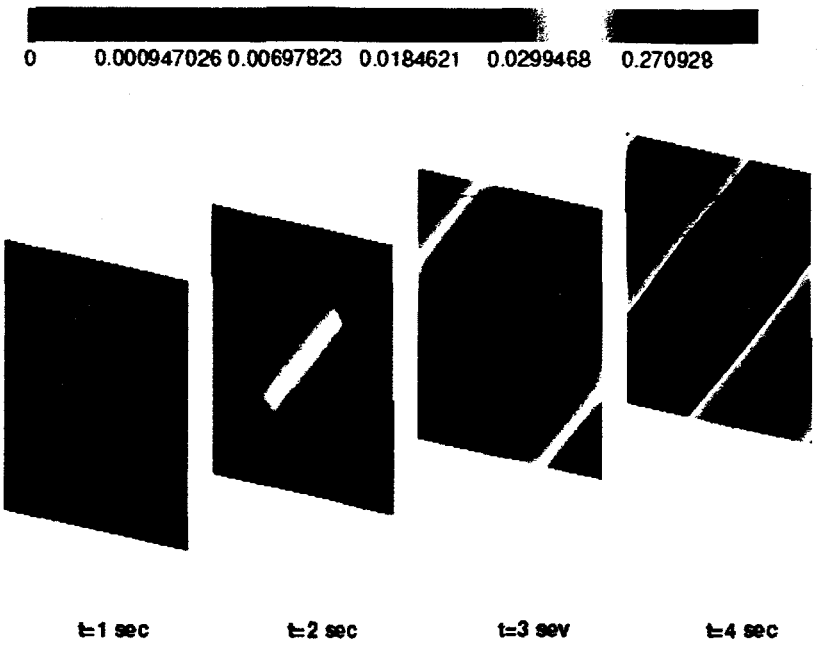

Figure 5.3.4. Coefficients of Thermal Design Sensitivity with Respect to Thermal Conductivity; $\frac{\partial u(x_c, y_c)}{\partial b_i}$; i =1 to 10.

Appendix I

Polynomials for Temperature Interpolation (up to 6 order) in XY_Plane

$$T = (\phi \otimes \theta \otimes \psi)^T a$$

Corner Functions

$\phi_1 = L_1$
$\phi_2 = L_2$
$\phi_3 = L_3$

Edge Functions: (P_{ip}-1) per edge

$$\phi_{1e} = -\sqrt{6} \cdot L_j \cdot L_k$$

$$\phi_{2e} = -\sqrt{10} \cdot \left(L_J \cdot L_K^2 - L_J^2 \cdot L_K\right)$$

$$\phi_{3e} = -\sqrt{\frac{7}{8}} \cdot \left(5 \cdot L_J \cdot L_K^3 - 10 \cdot L_J^2 \cdot L_K^2 + 5 \cdot L_J^3 \cdot L_K - L_J \cdot L_K\right)$$

$$\phi_{4e} = \frac{3}{2 \cdot \sqrt{2}} \cdot \left(-7 \cdot L_J \cdot L_K^4 + 21 \cdot L_J^2 \cdot L_K^3 - 21 \cdot L_J^3 \cdot L_K^2 + 7 \cdot L_J^4 \cdot L_K + 3 \cdot L_J \cdot L_K^2 - 3 \cdot L_J^2 \cdot L_K\right)$$

$$\phi_{5e} = \frac{\sqrt{11}}{4 \cdot \sqrt{2}} \cdot \left(-21 \cdot L_J \cdot L_K^5 + 84 \cdot L_J^2 \cdot L_K^4 - 126 \cdot L_J^3 \cdot L_K^3 + 84 \cdot L_J^4 \cdot L_K^2 - 21 \cdot L_J^5 \cdot L_K \right.$$
$$\left. + 14 \cdot L_J \cdot L_K^3 - 28 \cdot L_J^2 \cdot L_K^2 + 14 \cdot L_J^3 \cdot L_K - L_J \cdot L_K \right)$$

e	j	k
1	1	2
2	2	3
3	3	1

Permutation table for edge number, e, and corner points, j and k.

Bubble Functions: $(P_{ip}-1)*(P_{ip}-2)/2$

$$\phi_{1B} = L_1 \cdot L_2 \cdot L_3$$
$$\phi_{2B} = L_1 \cdot L_2 \cdot L_3 \cdot (L_2 - L_1)$$
$$\phi_{3B} = L_1 \cdot L_2 \cdot L_3 \cdot (2 \cdot L_3 - 1)$$
$$\phi_{4B} = L_1 \cdot L_2 \cdot L_3 \cdot (L_2 - L_1) \cdot (2 \cdot L_3 - 1)$$
$$\phi_{5B} = L_1 \cdot L_2 \cdot L_3 \cdot \frac{1}{2} \cdot \left(3 \cdot (L_2 - L_1)^2 - 1\right)$$
$$\phi_{6B} = L_1 \cdot L_2 \cdot L_3 \cdot \frac{1}{2} \cdot \left(3 \cdot (2 \cdot L_3 - 1)^2 - 1\right)$$
$$\phi_{7B} = L_1 \cdot L_2 \cdot L_3 \cdot \frac{1}{2} \cdot \left(3 \cdot (L_2 - L_1)^2 - 1\right) \cdot (2 \cdot L_3 - 1)$$
$$\phi_{8B} = L_1 \cdot L_2 \cdot L_3 \cdot (L_2 - L_1) \cdot \frac{1}{2} \cdot \left(3 \cdot (2 \cdot L_3 - 1)^2 - 1\right)$$
$$\phi_{9B} = L_1 \cdot L_2 \cdot L_3 \cdot \frac{1}{2} \cdot \left(5 \cdot (L_2 - L_1)^3 - 3 \cdot (L_2 - L_1)\right)$$
$$\phi_{10B} = L_1 \cdot L_2 \cdot L_3 \cdot \frac{1}{2} \cdot \left(5 \cdot (2 \cdot L_3 - 1)^3 - 3 \cdot (2 \cdot L_3 - 1)\right)$$

Appendix II

Lengendre Polynomials for Temperature Interpolation (up to 6 order) in Time

Lengendre Polynomials $(-1 \le \tau \le 1)$

$$\theta_0 = 1$$

$$\theta_1 = \tau$$

$$\theta_2 = \frac{1}{2}\left(3 \cdot \tau^2 - 1\right)$$

$$\theta_3 = \frac{1}{2}\left(5\tau^3 - 3\tau\right)$$

$$\theta_4 = \frac{1}{8}(35\tau^4 - 30\tau^2 + 3)$$

$$\theta_5 = \frac{1}{8}(63\tau^5 - 70\tau^3 + 15\tau)$$

$$\theta_6 = \frac{1}{16}(231\tau^6 - 315\tau^4 + 105\tau^2 - 5)$$

Appendix III

Polynomials for Temperature Interpolation (up to 6 order) through Thickness in Z

Integration of Legendre Polynomials $(-1 \le z \le 1)$

$$\psi_0 = \frac{1}{2}(1-z)$$

$$\psi_1 = \frac{1}{2}(1+z)$$

$$\psi_2 = \frac{1}{\sqrt{6}}(\frac{3}{2}\cdot z^2 - \frac{3}{2})$$

$$\psi_3 = \frac{1}{\sqrt{10}}(\frac{5}{2}z^3 - \frac{5}{2}z)$$

$$\psi_4 = \frac{1}{\sqrt{14}}(\frac{35}{8}z^4 - \frac{42}{8}z^2 + \frac{7}{8})$$

$$\psi_5 = \frac{1}{\sqrt{18}}(\frac{63}{8}z^5 - \frac{90}{8}z^3 + \frac{27}{8}z)$$

$$\psi_6 = \frac{1}{\sqrt{22}}(\frac{231}{16}z^6 - \frac{385}{16}z^4 + \frac{165}{16}z^2 - \frac{11}{16})$$

Appendix IV

Lagrange's Polynomials for Interpolation of Material Properties in XY Plane

Order 1,

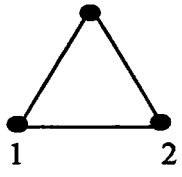

Corners

$$N_{p1} = L_1$$
$$N_{p2} = L_2$$
$$N_{p3} = L_3$$

Order 2,

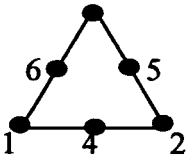

Corners

$$N_{p1} = (2 \cdot L_1 - 1) \cdot L_1$$
$$N_{p2} = (2 \cdot L_2 - 1) \cdot L_2$$
$$N_{p3} = (2 \cdot L_3 - 1) \cdot L_3$$

Mid-points

$$N_{p4} = 4 \cdot L_1 L_2$$
$$N_{p5} = 4 \cdot L_2 L_3$$
$$N_{p6} = 4 \cdot L_3 L_1$$

Order 3,

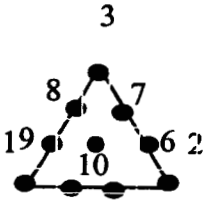

Corners

$$N_{p1} = \frac{1}{2}(3 \cdot L_1 - 1) \cdot (3 \cdot L_1 - 2) \cdot L_1$$

$$N_{p2} = \frac{1}{2}(3 \cdot L_2 - 1) \cdot (3 \cdot L_2 - 2) \cdot L_2$$

$$N_{p3} = \frac{1}{2}(3 \cdot L_3 - 1) \cdot (3 \cdot L_3 - 2) \cdot L_3$$

Mid-points

$$N_{p4} = \frac{9}{2} \cdot L_1 L_2 (3 \cdot L_1 - 1)$$

$$N_{p5} = \frac{9}{2} \cdot L_1 L_2 (3 \cdot L_2 - 1)$$

$$N_{p6} = \frac{9}{2} \cdot L_2 L_3 (3 \cdot L_2 - 1)$$

$$N_{p7} = \frac{9}{2} \cdot L_2 L_3 (3 \cdot L_3 - 1)$$

$$N_{p8} = \frac{9}{2} \cdot L_3 L_1 (3 \cdot L_3 - 1)$$

$$N_{p9} = \frac{9}{2} \cdot L_3 L_1 (3 \cdot L_1 - 1)$$

Center

$$N_{p10} = 27 \cdot L_1 L_2 L_3$$

Order 4,

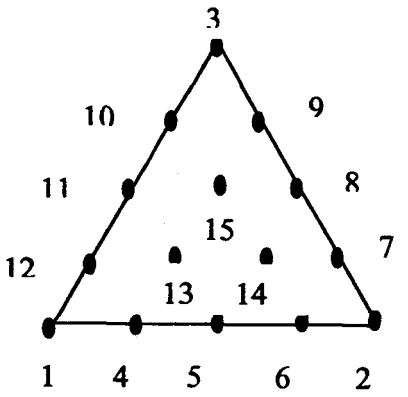

Corners

$$N_{p1} = \frac{1}{3}(4 \cdot L_1 - 1) \cdot (2 \cdot L_1 - 1) \cdot (4 \cdot L_1 - 3) L_1$$

$$N_{p2} = \frac{1}{3}(4 \cdot L_2 - 1) \cdot (2 \cdot L_2 - 1) \cdot (4 \cdot L_2 - 3) \cdot L_2$$

$$N_{p3} = \frac{1}{3}(4 \cdot L_3 - 1) \cdot (2 \cdot L_3 - 2) \cdot (4 \cdot L_3 - 3) \cdot L_3$$

Mid-points

$$N_{p4} = \frac{16}{3} \cdot L_1 L_2 (4 \cdot L_1 - 1) \cdot (2 \cdot L_1 - 1)$$

$$N_{p5} = 4 \cdot L_1 L_2 (4 \cdot L_1 - 1) \cdot (4 \cdot L_2 - 1)$$

$$N_{p6} = \frac{16}{3} \cdot L_1 L_2 (4 \cdot L_2 - 1) \cdot (2 \cdot L_2 - 1)$$

$$N_{p7} = \frac{16}{3} \cdot L_2 L_3 (4 \cdot L_2 - 1) \cdot (2 \cdot L_2 - 1)$$

$$N_{p8} = 4 \cdot L_2 L_3 (4 \cdot L_2 - 1) \cdot (4 \cdot L_3 - 1)$$

$$N_{p9} = \frac{16}{3} \cdot L_2 L_3 (4 \cdot L_3 - 1) \cdot (2 \cdot L_3 - 1)$$

$$N_{p10} = \frac{16}{3} \cdot L_3 L_1 (4 \cdot L_3 - 1) \cdot (2 \cdot L_3 - 1)$$

$$N_{p11} = 4 \cdot L_3 L_1 (4 \cdot L_3 - 1) \cdot (4 \cdot L_1 - 1)$$

$$N_{p12} = \frac{16}{3} \cdot L_3 L_1 (4 \cdot L_1 - 1) \cdot (2 \cdot L_1 - 1)$$

Center

$$N_{p13} = 32 \cdot L_1 L_2 L_3 (4 \cdot L_1 - 1)$$

$$N_{p14} = 32 \cdot L_1 L_2 L_3 (4 \cdot L_2 - 1)$$

$$N_{p15} = 32 \cdot L_1 L_2 L_3 (4 \cdot L_3 - 1)$$

Appendix V

Lagrange's Polynomials for Interpolation of Material Properties in Time and Through-Thickness

1st order

$$N(\xi) = N_0(\xi)\cdot u_0 + N_1(\xi)\cdot u_1$$

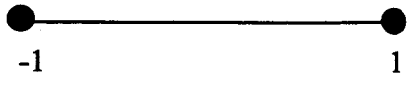

$$N_0(\xi) = \frac{1}{2}\cdot(1-\xi)$$

$$N_1(\xi) = \frac{1}{2}\cdot(1+\xi)$$

2nd order

$$N(\xi) = N_0(\xi)\cdot u_0 + N_1(\xi)\cdot u_1 + N_2(\xi)\cdot u_2$$

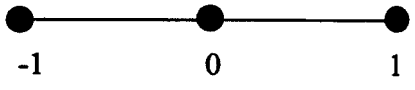

$$N_0(\xi) = \frac{3}{2}\cdot(-1+\xi)$$

$$N_1(\xi) = \frac{3}{2}\cdot(1+\xi)$$

$$N_2(\xi) = 1-\xi^2$$

3rd order

$$N(\xi) = N_0(\xi)\cdot u_0 + N_1(\xi)\cdot u_1 + N_2(\xi)\cdot u_2 + N_3(\xi)\cdot u_3$$

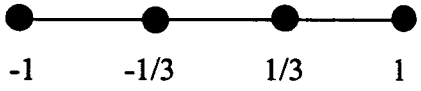

$$N_0(\xi) = \frac{1}{16}\cdot\left(-1+\xi+9\cdot\xi^2-9\cdot\xi^3\right)$$

$$N_1(\xi) = \frac{-1}{16}\cdot\left(1+\xi-9\cdot\xi^2-9\cdot\xi^3\right)$$

$$N_2(\xi) = \frac{1}{16}\cdot\left(9-27\cdot\xi-9\cdot\xi^2+27\cdot\xi^3\right)$$

$$N_3(\xi) = \frac{1}{16}\cdot\left(9+27\cdot\xi-9\cdot\xi^2-27\cdot\xi^3\right)$$

4th order

$$N(\xi) = N_0(\xi)\cdot u_0 + N_1(\xi)\cdot u_1 + N_2(\xi)\cdot u_2 + N_3(\xi)\cdot u_3 + N_4(\xi)\cdot u_4$$

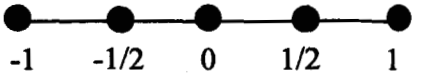

$$N_0(\xi) = \frac{1}{6}\cdot\left(\xi - \xi^2 - 4\cdot\xi^3 + 4\cdot\xi^4\right)$$

$$N_1(\xi) = \frac{-1}{6}\cdot\left(\xi + \xi^2 - 4\cdot\xi^3 - 4\cdot\xi^4\right)$$

$$N_2(\xi) = \frac{-1}{6}\cdot\left(8\cdot\xi - 16\cdot\xi^2 - 4\cdot\xi^3 + 16\cdot\xi^4\right)$$

$$N_3(\xi) = \frac{1}{6}\cdot\left(8\cdot\xi + 16\cdot\xi^2 - 4\cdot\xi^3 - 16\cdot\xi^4\right)$$

$$N_4(\xi) = \left(1 - 5\cdot\xi^2 + 4\cdot\xi^4\right)$$

5th order

$$N(\xi) = N_0(\xi)\cdot u_0 + N_1(\xi)\cdot u_1 + N_2(\xi)\cdot u_2 + N_3(\xi)\cdot u_3 + N_4(\xi)\cdot u_4 + N_5(\xi)\cdot u_5$$

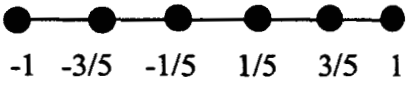

$$N_0(\xi) = \frac{1}{768}\cdot\left(9 - 9\cdot\xi - 250\cdot\xi^2 + 250\cdot\xi^3 + 625\cdot\xi^4 - 625\cdot\xi^5\right)$$

$$N_1(\xi) = \frac{1}{768}\cdot\left(9 + 9\cdot\xi - 250\cdot\xi^2 - 250\cdot\xi^3 + 625\cdot\xi^4 + 625\cdot\xi^5\right)$$

$$N_2(\xi) = \frac{-1}{768}\cdot\left(75 - 125\cdot\xi - 1950\cdot\xi^2 + 3250\cdot\xi^3 + 1875\cdot\xi^4 - 3125\cdot\xi^5\right)$$

$$N_3(\xi) = \frac{-1}{768}\cdot\left(75 + 125\cdot\xi - 1950\cdot\xi^2 - 3250\cdot\xi^3 + 1875\cdot\xi^4 + 3125\cdot\xi^5\right)$$

$$N_4(\xi) = \frac{1}{768}\cdot\left(450 - 2250\cdot\xi - 1700\cdot\xi^2 + 8500\cdot\xi^3 + 1250\cdot\xi^4 - 6250\cdot\xi^5\right)$$

$$N_5(\xi) = \frac{1}{768}\cdot\left(450 + 2250\cdot\xi - 1700\cdot\xi^2 - 8500\cdot\xi^3 + 1250\cdot\xi^4 + 6250\cdot\xi^5\right)$$

Appendix VI

Sample Matrices for Analysis and Sensitivity Analysis

$$C_{\Omega_e} = \int_{t_{n-1}}^{t_n} \int_{\Omega_p} \int_{\frac{-d}{2}}^{\frac{d}{2}} \rho c \chi \frac{\partial \chi^T}{\partial t} dz dA dt$$

$$= \int_{t_{n-1}}^{t_n} \int_{\Omega_e} \int_{\frac{-d}{2}}^{\frac{d}{2}} (N_c^T \delta_c)(\varphi \otimes \psi \otimes \theta)\left(\varphi \otimes \psi \otimes \frac{d\theta}{dt}\right)^T dz dA dt \qquad \text{(VI.1)}$$

$$= \sum_i \sum_j \sum_k \{ (\int_{\Omega_p} \varphi \varphi^T N_{cpi} dA \otimes \int_{\frac{-d}{2}}^{\frac{d}{2}} \psi \psi^T N_{czk} dz \otimes \int_{t_{n-1}}^{t_n} \theta \frac{d\theta^T}{dt} N_{cij} dt) \delta_{ijk} \}$$

$$J_{c,\Omega_p} = \int_{t_{n-1}}^{t_n} \int_{\Omega_p} \int_{\frac{-d}{2}}^{\frac{d}{2}} \frac{\partial(\rho c)}{\partial a}(\chi) \frac{\partial(\chi^T \cdot a)}{\partial t} dz dA dt$$

$$= \int_{t_{n-1}}^{t_n} \int_{\Omega_p} \int_{\frac{-d}{2}}^{\frac{d}{2}} N_c^T \frac{\partial \delta_c}{\partial a}(\varphi \otimes \psi \otimes \theta)\left(\varphi \otimes \psi \otimes \frac{d\theta}{dt}\right)^T a dz dA dt \qquad \text{(VI.2)}$$

$$= \sum_i \sum_j \sum_k \{[(\int_{\Omega_p} \varphi \varphi^T N_{cpi} dA \otimes \int_{\frac{-d}{2}}^{\frac{d}{2}} \psi \psi^T N_{czk} dz \otimes \int_{t_{n-1}}^{t_n} \theta \frac{d\theta^T}{dt} N_{cij} dt) a](\alpha_{ijk} \chi_{ijk})\}$$

$$\frac{dC_{\Omega_p}}{db} = \int_{t_{n-1}}^{t_n} \int_{\Omega_p} \int_{\frac{-d}{2}}^{\frac{d}{2}} \frac{\partial(\rho c)}{\partial b} \chi \frac{\partial \chi^T}{\partial t} dz dA dt$$

$$= \int_{t_{n-1}}^{t_n} \int_{\Omega_e} \int_{\frac{-d}{2}}^{\frac{d}{2}} (N_c^T \frac{\partial \delta_c}{\partial b})(\phi \otimes \psi \otimes \theta)\left(\phi \otimes \psi \otimes \frac{d\theta}{dt}\right)^T dz dA dt \qquad \text{(VI.3)}$$

$$= \sum_i \sum_j \sum_k \{ (\int_{\Omega_p} \phi \phi^T N_{cpi} dA \otimes \int_{\frac{-d}{2}}^{\frac{d}{2}} \psi \psi^T N_{czk} dz \otimes \int_{t_{n-1}}^{t_n} \theta \frac{d\theta^T}{dt} N_{cij} dt) \frac{\partial \delta_{ijk}}{\partial b} \}$$

Attachment I

Paper Presented at the 14th Annual Thermal and Fluids Analysis Workshop

August 18th-22nd, 2003

Hampton, Virginia

SENSITIVITY EQUATION DERIVATION FOR TRANSIENT HEAT TRANSFER PROBLEMS

By

Gene Hou and Ta-Cheng Chien
Department of Mechanical Engineering
Old Dominion University
Norfolk, VA 23529-0247

Jeenson Sheen
Department of Technology
Norfolk State University
Norfolk, VA 23504

ABSTRCT

The focus of the paper is on the derivation of sensitivity equations for transient heat transfer problems modeled by different discretization processes. Two examples will be used in this study to facilitate the discussion. The first example is a coupled, transient heat transfer problem that simulates the press molding process in fabrication of composite laminates. These state equations are discretized into standard *h*-version finite elements and solved by a multiple step, predictor-corrector scheme. The sensitivity analysis results based upon the direct and adjoint variable approaches will be presented. The second example is a nonlinear transient heat transfer problem solved by a *p*-version time-discontinuous Galerkin's Method. The resulting matrix equation of the state equation is simply in the form of $\boldsymbol{Ax} = \boldsymbol{b}$, representing a single step, time marching scheme. A direct differentiation approach will be used to compute the thermal sensitivities of a sample 2D problem.

INTRODUCTION

Sensitivity analysis is defined in this paper as a process that derives sensitivity equations to compute the derivatives of responses or states with respect to specified variables. Since the derivative information can greatly enhance the robustness and accuracy of curve fitting, sensitivity analysis becomes a necessary element in many engineering applications. Examples include design trade-off, weather prediction, analysis error correction, model adjustment, reliability analysis and design optimization.

In sensitivity analysis, the response or dependent variable can be a real number, a function or a functional and the independent variable can be a real number or a function. The challenge of sensitivity analysis arises when the responses to be differentiated involve the solutions of some governing equations. In these cases, the

responses or states are implicitly related to the independent variables through the governing equations. These governing state equations can be expressed as differential, integral or algebraic forms. The latter is usually as a result of numerical discretization of the former.

Many approaches are available for sensitivity analysis, including automatic differentiation[1], complex variable method[2], finite differencing, or more traditional analytical approaches[3-6]. The analytical approaches used for sensitivity analysis can be further classified into various categories. It can be classified as the discrete approach or the distributed (continuous) approach, based upon which types of governing equations, responses and independent variables are considered. The discrete approach works with discretized algebraic equations and real numbers, while the distributed approach works with functionals and functions. Sensitivity analysis can also be classified as the direct differentiation approach or the adjoint variable approach, based upon whether the derivatives of the state variables are computed explicitly in the process. The bulk of the effort of the direct differentiation method is to establish a sensitivity equation solved for the derivatives of state variables, whereas the effort of the adjoint approach is to form and solve an adjoint equation and eventually, compute the derivatives of the responses without explicitly computing the derivatives of the state variables.

Subjects related to sensitivity analysis of dynamic transient problems can be found in the literature [3-4,6] . Thermal transient analysis can be performed in the similar fashion[7-9]. Recent development and applications of thermal transient analysis can be found in aerospace applications[10-11], laser surface treatment[12], material processes[13-14], and their references. The major focus of the report is on the derivation of sensitivity equations for transient heat transfer problems represented in various forms of governing equations. Two examples will be used in this study to facilitate the discussion.

The first example is a coupled, transient heat transfer problem that simulates the press molding process in fabrication of composite laminates. The state equations are made of a heat conduction equation that calculates the through-thickness temperature distribution and an empirical equation that monitors the chemical-kinetic reaction of resins. These state equations are discretized into standard *h*-version finite elements and expressed in the form of $A\dot{x} + Bx = c$. The resultant equations are then solved by a multiple step, predictor-corrector scheme. Both of the direct and adjoint variable approaches will be used to derive the sensitivity equations in continuous forms. The numerical implementation aspects of those sensitivity equations and their accuracies will be studied in this paper.

The second example is a nonlinear transient heat transfer problem solved by a *p*-version, time-discontinuous Galerkin's Method[15-17]. The resulting matrix equation of the state equation is simply in the form of $Ax = b$, representing a single step, time marching scheme. A direct differentiation approach is used to compute the thermal

sensitivities of a simple 2 D heat conduction problem. Here, possible usages of the sensitivity results are presented.

EXAMPLE 1: *h*-VERSION FINITE ELEMENT APPROXIMATION

The interest of this study is in compression molding of a filled polyester resin reinforced by chopped glass fibers. The unmolded composite is produced in sheets which are from 3 to 6 mm thick, typically. The resin consists of a thick dough and the chopped fibers (about 25 mm long) which are randomly oriented in the plane of the sheet. In this form, the material is called sheet molding compound, or simply SMC[18]. A diffusion reaction system in terms of the temperature distribution and the degree of cure can be used to describe the cure process of the composite material under consideration.

The system equations can be expressed as

$$\rho c\frac{\partial u}{\partial t}-k\frac{\partial^2 u}{\partial x^2}=\rho H_r\frac{\partial \alpha}{\partial t}, \qquad \text{in} \quad (0,h)\times(0,\tau] \qquad (1)$$

$$u(h,t)=u_c(t) \qquad \text{on} \quad (0,\tau] \qquad (2)$$

$$\frac{\partial u(0,t)}{\partial x}=0 \qquad \text{on} \quad (0,\tau] \qquad (3)$$

and

$$u=u_0(x), \qquad \text{in} \quad (0,h) \text{ at } t=0 \qquad (4)$$

where ρ and c are the density and the specific heat of the composite material, respectively, k is the thermal conductivity in the direction perpendicular to the plane of composite material, $2h$ is the total thickness, $u_c(t)$ is the cure cycle in K°, τ is the time in seconds needed for the completion of one cure cycle, H_r is the total or ultimate heat of reaction, and the last term in Eq. 1, $\rho H_r \partial\alpha/\partial t$, is the rate of heat generated by the chemical reaction as characterized by the degree of cure α.

The degree of cure, α, is defined as the fraction of heat, $H(t)$, released up to time, t, for the resin system under cure; $\alpha = H(t)/H_r$. Both $H(t)$ and H_r in Eq. 4 can be measured experimentally by Differential Scanning Calorimetry (DSC). For an uncured material, α approaches zero, and for a completely cured material, α approaches one. The reaction rate, $\partial\alpha/\partial t$, depends strongly on the curing temperature. As an example, the cure rate equation of a stepwise isothermal curing process which can be used for a polyester SMC is described as follows:

$$\begin{aligned}\frac{\partial \alpha}{\partial t} &= f(\alpha, T) \\ &= (K_1 + K_2 \alpha^m)(1-\alpha)^n \\ &= (a_1 e^{-d_1/RT} + a_2 e^{-d_2/RT} \alpha^m)(1-\alpha)^n\end{aligned} \tag{5}$$

where a_1, a_2, d_1, d_2, m and n are constants, R is the universal gas constant, and K_1 and K_2 are exponential functions of the temperature.

The optimal cure cycle design[19] aims to select the profile of cure temperature, $u_c(t)$, to achieve the following goals in a compress molding process.

a) The maximum temperature inside the composite during the cure process can not be too high to avoid buring.
b) The material is cured completely at the end of the cure process.
c) The material is cured uniformly at any time during the cure process.

The first two objectives may be mathematically formulated as point-wise functions,

$$T(t) \le T_f \qquad \text{in} \qquad [0,h]\text{x}[0,\tau]$$

$$\alpha(x,\tau) \ge \alpha_f \qquad \text{in} \qquad [0,h]$$

where τ is the total time required to complete one cure cycle. Furthermore, the last objective may be measured by the temperature uniformity, which is expected to lead to the uniformity of the curing reaction. Mathematically, the temperature uniformity is represented by the least-square integral of the deviation between the point-wise temperature and the averaged temperature as

$$\psi_0 = \int_0^{\tau} [\int_0^{h} u^2 dx - (\int_0^{h} u dx)^2 / h] dt \tag{6}$$

To support the optimal cure cycle design, the thermal design derivatives of the functional, ψ_0, the temperature, $u(x,t)$ and the degree of cure, $\alpha(x,t)$, with respect to the cure temperature, $u_c(t)$, are required.

Note that the cure temperature appears as a part of the non-homogeneous boundary equation in Eq. 2. By using the following replacement of the temperature, $u(x, t)$, by $\bar{u}(x, t)$ as

$$u(x,t) = \bar{u}(x,t) + u_c(t) \tag{7}$$

which leads to simplification of the heat conduction equation, Eq. 1,

$$\rho c \frac{\partial \bar{u}}{\partial t} = k \frac{\partial^2 \bar{u}}{\partial x^2} - \rho c \frac{\partial u_c}{\partial t} + \rho H_r f(\alpha, \bar{u} + u_c)$$

with the homogeneous boundary equations

$$\bar{u}(h,t)=0, \qquad \text{in} \quad [0,\tau] \qquad (8)$$

$$\frac{\partial \bar{u}(0,t)}{\partial x}=0, \qquad \text{in} \quad [0,\tau] \qquad (9)$$

and the initial condition,

$$\bar{u}(x,0)=u_0(x)-u_c(0), \qquad \text{in} \quad [0,h] \qquad (10)$$

where f is defined in Eq. 5. Since the initial temperature, $u_0(t)$ is the same as the initial cure temperature for most applications, Eq. 10 may yield a homogeneous initial condition as well. From here on, $\bar{u}(x,t)$ is abbreviated as $u(x,t)$ for simplification.

The weak forms of the above equation can now be derived based upon the Galerkin's method for arbitrary functions, $w(x)$ and $s(x)$, as

$$\pi_u = 0 = \int_0^h \left(\rho c \frac{\partial u}{\partial t} - k \frac{\partial^2 u}{\partial x^2} + \rho c \frac{du_c}{dt} - \rho H_r f \right) w dz \qquad (11)$$

and

$$\pi_\alpha = 0 = \int_0^h \left(\frac{\partial \alpha}{\partial t} - f \right) s dx \qquad (12)$$

THERMAL SENSITIVITY ANALYSIS

The system equation of Eqs. 1-5 simply reveals the fact that their solutions, $u(x,t)$ and $\alpha(x,t)$ are functions of the design variable, $u_c(t)$. However, since the design variable $u_c(t)$ itself is a function, the thermal derivative of $u(x,t)$ with respect to $u_c(t)$ can be defined as the variation of $u(x,t)$, δu, due to the variation in $u_c(t)$, δu_c,

$$\delta u = \frac{d}{d\varepsilon} u(x,t;u_c+\varepsilon \delta u_c)\Big|_{\varepsilon=0}$$

The cure derivative, $\delta\alpha$ can be defined similarly.

The variation of the functional defined in Eq. 6 is then given as

$$\delta\psi = \int_0^\tau \left[\int_0^h 2u - \frac{2}{h} \int_0^h u dx \right] \delta u dx dt \qquad (13)$$

It is assumed that $u(x,t;u_c)$ and $\alpha(x,t;u_c)$ have enough regularity in the time-spatial domain and in the design space. Thus, the order of the differentiation and the variation is exchangeable; therefore,

$$\frac{\partial(\delta u)}{\partial t} = \delta\left(\frac{\partial u}{\partial t}\right)$$
$$\frac{\partial(\delta \alpha)}{\partial t} = \delta\left(\frac{\partial \alpha}{\partial t}\right)$$

and

$$\frac{\partial^2(\delta u)}{\partial x^2} = \delta\left(\frac{\partial^2 u}{\partial x^2}\right)$$

With the aid of the above equations, the variations of the state equations defined by Eq. 11 - 12 yield

$$0 = \int_0^\tau \int_0^h \left(\rho c \frac{\partial \delta u}{\partial t}\lambda + \rho c \frac{d(\delta u_c)}{dt}\lambda - \rho \frac{\partial^2(\delta u)}{\partial x^2}\lambda - \rho H_r \frac{\partial f}{\partial \alpha}\delta\alpha\lambda - \rho H_r \frac{\partial f}{\partial u}\delta u\lambda - \rho H_r \frac{\partial f}{\partial u_c}\delta u_c\lambda \right) dx dt, \tag{14}$$

and

$$0 = \int_0^\tau \int_0^h \left(s\delta\frac{\partial(\delta\alpha)}{\partial t} - s\frac{\partial f}{\partial \alpha}\delta\alpha - s\frac{\partial f}{\partial u}\delta u - s\frac{\partial f}{\partial u_c}\delta u_c \right) dx dt. \tag{15}$$

Integrating by parts simplify the above equation as

$$0 = \int_0^\tau \int_0^h \left[\left(-\rho c\frac{\partial \lambda}{\partial t} - k\frac{\partial^2 \lambda}{\partial x^2} - \rho H_r \lambda \frac{\partial f}{\partial u} \right)\delta u + \left(-\rho c\frac{\partial \lambda}{\partial t} - \rho H_r \lambda \frac{\partial f}{\partial u_c} \right)\delta u_c - \rho H_r \lambda \frac{\partial f}{\partial \alpha}\delta\alpha \right] dx dt + \int_0^\tau k\frac{\partial \lambda}{\partial x}\delta u \Big|_0^h dt - \int_0^\tau k\lambda \frac{\partial(\delta u)}{\partial x}\Big|_0^h dt + \int_0^h \rho c\lambda \delta u \Big|_0^\tau dx + \int_0^h \rho c\lambda \delta u_c \Big|_0^\tau dx, \tag{16}$$

and

$$0 = \int_0^{\tau}\int_0^{h}\left(-\frac{\partial s}{\partial t}\delta\alpha - s\frac{\partial f}{\partial \alpha}\delta\alpha - s\frac{\partial f}{\partial u}\delta u - s\frac{\partial f}{\partial u_c}\delta u_c\right)dxdt + \int_0^{h} s\delta\alpha\Big|_0^{\tau} dx. \tag{17}$$

THE ADJOINT VARIABLE APPROACH

Adding Eqs. 13, 16, and 17 up, one has the variation of the functional ψ as

$$\begin{aligned}\delta\psi = &\int_0^{\tau}\int_0^{h}\left[\left(2u - \frac{2}{h}\int_0^{h} u dz\right) - \rho c\frac{\partial\lambda}{\partial t} - k\frac{\partial^2\lambda}{\partial x_2} - \rho H_r\frac{\partial f}{\partial u} - s\frac{\partial f}{\partial u}\right]\delta u dx dt \\ &+ \int_0^{\tau}\int_0^{h}\left(-\rho H_r\lambda\frac{\partial f}{\partial \alpha} - \frac{\partial s}{\partial t} - s\frac{\partial f}{\partial \alpha}\right)\delta\alpha dx dt \\ &+ \int_0^{\tau}\int_0^{h}\left(-\rho c\frac{\partial\lambda}{\partial t} - \rho H_r\lambda\frac{\partial f}{\partial u_c} - s\frac{\partial f}{\partial u_c}\right)\delta u_c dx dt \\ &+ \int_0^{h}\rho c\lambda\delta u_c\Big|_0^{\tau} + \int_0^{\tau} k\frac{\partial\lambda}{\partial x}\delta u\Big|_0^{h} dt - \int_0^{\tau} k\lambda\frac{\partial\delta u}{\partial x}\Big|_0^{h} dt \\ &+ \int_0^{h}\rho c\lambda\delta u_c\Big|_0^{\tau} dx + \int_0^{h} s\delta\alpha\Big|_0^{\tau} dx\end{aligned} \tag{18}$$

Note that $\lambda(x,t)$ and $s(x,t)$ are arbitrary functions, and the design derivatives δu and $\delta\alpha$ are the only two unknowns in the above equation. One may now specify the variables λ and s in such a way that all of the terms associated with δu and $\delta\alpha$ are dropped. This can be accomplished by introducing the following adjoint equations for λ and s as:

$$0 = \rho c\frac{\partial\lambda}{\partial t} + k\frac{\partial^2\lambda}{\partial x^2} + \rho H_r\frac{\partial f}{\partial u} + s\frac{\partial f}{\partial u} - \left(2u - \frac{2}{h}\int_0^{h} u dx\right) \tag{19}$$

and

$$0 = \frac{\partial s}{\partial t} + \rho H_r\lambda\frac{\partial f}{\partial \alpha} + s\frac{\partial f}{\partial \alpha} \tag{20}$$

with the terminal conditions,

$$\lambda(0,\tau) = 0, \qquad \text{in} \qquad [0, h] \tag{21}$$

$$s(x,\tau)=0, \qquad \text{in} \qquad [0,h] \tag{22}$$

and the boundary conditions,

$$\frac{\partial\lambda}{\partial x}(0,t)=0, \qquad \text{in} \qquad [0,\tau] \tag{23}$$

$$\lambda(h,t)=0, \qquad \text{in} \qquad [0,\tau] \tag{24}$$

Thus, the combination of Eqs, 18 - 24 provides a simple formula for the design derivative of the functional,

$$\begin{aligned}\delta\psi = &\int_0^{\tau}\int_0^{h}\left(-\rho c\frac{\partial\lambda}{\partial t}-\rho H_r\frac{\partial f}{\partial u_c}-s\frac{\partial f}{\partial u_c}\right)\delta u_c\,dx\,dt \\ &+\int_0^{h}\rho c\lambda(0)\delta u_c(0)\,dx\end{aligned} \tag{25}$$

Equation 25 shows that the design derivative of ψ, namely, $\delta\psi$, is a functional of state variables α and u, and the adjoint variables λ and s. The matrix equations which solve the nodal values of α and u can be formed by the standard h-version finite element method as.

$$C\dot{a}+Ka=q \tag{26}$$

$$M\dot{\alpha}=r \tag{27}$$

Since the adjoint variables of Eqs. 19 – 20 form an "adjoint" diffusion-reaction system similar to the original one, the same numerical scheme used to solved the state variables α and u can be extended here to compute the adjoint variables λ and s. For instance, using the same shape functions of u and α to interpolate the adjoint variables λ and s obtains the following matrix equation for nodal value of λ and s in the form of

$$C\dot{\lambda}-K\lambda=q^{*} \tag{28}$$

and

$$M\dot{s}=r^{*} \tag{29}$$

with proper boundary and terminal conditions.

In general, the adjoint equation cannot be solved simultaneously alongside with the original system equation. Because of the terminal conditions, the adjoint equations can be solved by either the backward integration along the real time t – axis directly or the forward integration along the artificial time t^{*} - axis, provided that the

independent variable t is changed to t^* ax $t^* = \tau - t$. However, both approaches require the solution of the original system equation known prior to solving the adjoint equations.

THE DIRECT DIFFERENTIATION METHOD

The direct differentiation method is an approach that differentiates the governing equations with respect to a design variable directly. The variation δu in $\delta\psi$ of Eq. 13 and $\delta\alpha$ can be obtained by solving the equations, $\delta\pi_\alpha = 0$ and $\delta\pi_u = 0$, in their weak forms such as Eqs. 14-15, or in their differential forms as

$$\rho c\frac{\partial(\delta u)}{\partial t} = k\frac{\partial^2(\delta u)}{\partial x^2} - \rho c\frac{\partial(\delta uc)}{\partial t} + \rho H_r\frac{\partial f}{\partial \alpha}\delta\alpha + \rho H_r\frac{\partial f}{\partial u}\delta u + \rho H_r\frac{\partial f}{\partial u_c}\delta u_c \tag{30}$$

and

$$\frac{\partial(\delta\alpha)}{\partial t} = \frac{\partial f}{\partial \alpha}\delta\alpha + \frac{\partial f}{\partial u}\delta u + \frac{\partial f}{\partial u_c}\delta u_c \tag{31}$$

where the design variable variation, δu_c, is known.

Again, Eqs. 14-15 or Eqs. 30-31 can be discretized into finite element matrix equations, similar to Eqs. 26-27 as δu and $\delta\alpha$ can be interpolated by the same shape functions as u and α. These equations can be symbolically written as

$$C\dot{\boldsymbol{a}}_b + K\boldsymbol{a}_b = \boldsymbol{q}_b \tag{32}$$

$$M\dot{\boldsymbol{\alpha}}_b = \boldsymbol{r}_b \tag{33}$$

where δu and $\delta\alpha$ are interpolated by the same shape functions as u and α, in which $\boldsymbol{a}_b$ and $\boldsymbol{\alpha}_b$ are the nodal vectors of δu and $\delta\alpha$.

NUMERICAL RESULTS

The initial-value problems of the state variables, their thermal derivatives and corresponding adjoint variables are all solved by the computer code, DE[20]. The DE program is one of predictor-corrector integration algorithms using Adams family of

formulas. The truncation error is controlled by varying both the step size and the order of the polynomial approximation. The DE program is quite easy to use and has the capability to manage moderate stiff equations which happen commonly in the problems of chemical kinetics. To maintain a unified accuracy in the analysis, the computation of two state variables, namely, the temperature and the degree of cure, are subjected to the same error tolerance in this study.

Note that the coefficient matrices of a_b and α_b in Eqs. 32-33 are identical to those of a and α defined in Eqs. 26-27. Therefore, the same numerical scheme and the numerical tolerance can be applied to solve both Eq. 26-27, and 32-33 simultaneously for state variables, a and α, and design derivatives, a_b and α_b. In this way, the state variables and the design derivatives can enjoy the same numerical accuracy.

Regarding the computational efficiency, it is worthwhile mentioning two notes here:
a) Because the coefficient matrices of Eqs. 32-33 are identical to those of Eqs. 26-27, the triangular factorizations of matrices C and M are needed to be done only once.
b) Compared to the original system equations, the right hand sides of the equations for computing a_b and α_b, such as Eqs. 32-33, may have different frequency contents. Thus, to maintain the same numerical accuracy, a small time step Δt may be required for the DE program to solve the pairs (a,α) and (a_b,α_b), simultaneously.
Once a and a_b are available, the design derivative given in Eq. 13 can be easily obtained by numerical integration. Another suggestion is to rewrite the integral form of Eq. 13 as a differential equation of $\delta\psi$ given as

$$\frac{d\delta\psi}{dt} = \int_0^h \left[2u - \frac{2}{h}\int_0^h u dz \right] \delta u dz \tag{34}$$

The above ordinary differential equation of $\delta\psi_b$ can then be solved simultaneously with equations of (a,α) and (a_b,α_b). In this way, one extra equation of design derivative $\delta\psi$ for each design variable is added in the design sensitivity analysis. However, the accuracy of $\delta\psi$ is secured. Eq. 34 is used to generate the current numerical results.

An example which deals with the cure process of compression molding is presented in this section to discuss the numerical accuracy of the adjoint variable method and the direct differentiation method for calculating the thermal design derivatives. The accuracy of the thermal design sensitivity can be checked by using the fundamental definition of design derivatives which can be approximated by the finite difference.

The finite perturbation of the design variable, Δb, is defined as the difference between a perturbed design b^* and the nominal design b, i.e., $\Delta b = b^* - b$. As a result, it follows that

$$\begin{aligned} \Delta\psi &= \psi(b^*) - \psi(b) \\ &\cong \psi' \Delta b \end{aligned} \tag{35}$$

The above equation provides a simple means to check the accuracy of the design sensitivity analysis. Nevertheless, the difficulty of this method is the selection of Δb. If Δb is too large, the approximation in Eq. 35 is not valid. On the other hand, if Δb is too small, the round-off error in the computation of $[\psi(b^*) - \psi(b)]$ becomes too large to ensure the validity of Eq. 35.

The first example present here deals with the cure process in which the cure temperature of the process is assumed to be a constant temperature. The nominal cure temperature is taken as 423°k. According to the approximation defined in Eq. 35, the results of $\Delta\psi$ and Δb shown in Fig. 1 demonstrate that the thermal design sensitivity calculated by the direct differentiation method is more accuracy than the results calculated by adjoint variable method. Moreover, by using the direct differentiation method, one can also get the time histories of the design derivatives of state variables as shown in Figs. 2 and 3.

EXAMPLE 2: *p*-VERSION, TIME-DISCONTINIOUS FINITE ELEMENT APPROXIMATION

This example will examine a more general heat conduction equation than the one presented in Eq. 1. The governing differential equation is given as

$$\rho c \frac{\partial u}{\partial t} - \sum_{i=1}^{3} \sum_{j=1}^{3} \frac{\partial}{\partial x_i} \left[k_{ij} \frac{\partial u}{\partial x_j} \right] = Q(x,t), \quad \text{in } \Omega \times (0,T] \tag{36}$$

$$u = f(x,t) \qquad \text{on } \partial\Omega_u \times (0,T] \tag{37}$$

$$\sum_{i=1}^{3} \sum_{j=1}^{3} k_{ij} \frac{\partial u}{\partial x_j} [n_i] = q_s(x,t), \qquad \text{on } \partial\Omega_q \times (0,T] \tag{38}$$

$$\sum_{i=1}^{3} \sum_{j=1}^{3} k_{ij} \frac{\partial u}{\partial x_j} [n_i] = -h(u - T_\infty), \qquad \text{on } \partial\Omega_h \times (0,T] \tag{39}$$

and

$$u = g(x), \qquad \text{in } \Omega \text{ at } t = 0 \tag{40}$$

where the temperature, u(x,t), is the only unknown. Eq. 36 represents an initial-boundary value problem with Eqs.37-39 being the temperature, the heat flux

boundary condition, and the thermal convective condition; respectively, and Eq. 40, the initial conditions. It is assumed that the heat source, Q, the prescribed temperature, f, the flux, q_s, the thermal film coefficient, h, and the initial value, g, are all with proper regularity. In case of material nonlinearity, the specific heat, ρc(u), the film coefficient, $h(u)$, and the thermal conductivity, k_{ij}(u) are assumed to be functions of temperature.

Let $f = 0$ on Ω_u. Otherwise, u in Eqs.36-40 can be replaced by $u - f$ to achieve a homogenous boundary condition on Ω_u. As a result, the weak form of Eqs. 36-40 can be derived, based upon the Galerkin's Method for an arbitrary function, $w(x)$, as

$$\int_{\Omega}(\rho c\frac{\partial u}{\partial t}w+\sum_{i-1}^{3}\sum_{j=1}^{3}k_{ij}\frac{\partial u}{\partial x_i}\frac{\partial w}{\partial x_j})dv+\int_{\partial\Omega_h}huwds$$

$$=\int_{\Omega}Qwdv+\int_{\partial\Omega_q}q_swds+\int_{\partial\Omega_h}hT_\infty wds \tag{41}$$

In the approach of time-discontinuous Galerkin's method that is under development in this study, the time coordinate is treated as the same as the spatial coordinate. The time space is also discretized into elements or intervals. Focusing on one time interval, $I_n = [t_{n-1}, t_n)$, the weak form, Eq. 41, can be extended to the entire product domain $I_n \times \Omega$

$$\int_{n-1}^{n}[\int_{\Omega}\rho c\frac{\partial u}{\partial t}w+\sum_{i=1}^{3}\sum_{j=1}^{3}k_{ij}\frac{\partial u}{\partial x_i}\frac{\partial w}{\partial x_j})dv\,]dt+\int_{n-1}^{n}[\int_{\partial\Omega_h}huwds\,]dt$$

$$=\int_{n-1}^{n}[\int_{\Omega}Qwdv+\int_{\partial\Omega_q}q_swds+\int_{\partial\Omega_h}hT_\infty wds]dt \tag{42}$$

where, $w(x,t)$ is the testing function. Furthermore, to enforce the continuous requirement at the interfaces of time intervals, a weighted integral form of constraint, is appended to Eq. 42

$$\int_{\Omega}(\rho c^{+}u^{+}-\rho c^{-}u^{-})w^{+}dv=0 \tag{43}$$

In this example, the temperature, $u(x, t)$, is interpolated by a p-version hierarchical basis functions as

$$u(x,t)=\chi^{T}(x,y,z,t)a$$
$$=(\phi(x,y)\otimes\psi(z)\otimes\theta(t))^{T}a \tag{44}$$

The symbol, $\otimes$, represents the outer tensor product operator and the vectors, ϕ, ψ and θ, represent collections of basis functions. Particularly, the through-thickness basis functions, ψ, are made of the Legendre polynomials of the first kind[15], the temporal basis functions, θ, the integrations of the same Legendre polynomials and the in-plane basis functions, ϕ, chosen for triangular elements, as described by reference 21.

It is assumed that in this study, the film coefficient h is set to zero and the relations between the other material properties, ρc and K_{ij}, and the temperature are defined in a tabulated form, presented as a result of experiments. Therefore, the material properties cannot be explicitly specified as functions of position and time as required by integration. An approximation is thus introduced to overcome such a difficulty. The standard Lagrange polynomials are used here for this purpose.

The values of the material properties at the Lagrange points are taken from a given material table based upon the values of the temperature found at those points. The values of the material properties at elsewhere in an element are then obtained through interpolation. In this way, the material properties can be explicitly approximated as functions of position and time throughout the problem domain.

As an example, the material property, say ρc, can be interpolated in an element $(I_n \times \Omega_p)$ as

$$\begin{aligned} \rho c(x,t) &= (N_c(x,y,z,t))^T \delta_c \\ &= (N_{cp}(x,y) \otimes N_{cz}(z) \otimes N_{ct}(t))^T \delta_c \\ &= \sum_i \sum_j \sum_k \; (N_{cpi}(x_i,y_i) \otimes N_{czj}(z_j) \otimes N_{ctk}(t_k))^T \delta_{cijk} \end{aligned} \tag{45}$$

where, δ_{cijk} is a component of the vector, δ_c, which takes the value of the material properties found in the material table.

If the material properties are interpolated linearly through the tabulated data, the value of the materials can be represented as, using ρc as an example,

$$\delta_{cijk} = \alpha_{ijk} + \beta_{ijk} u_{ijk}$$

where α_{ijk} and β_{ijk} are constants taken from the material table based upon the temperature value, u_{ijk}, measured at the location (x_i, y_i, z_j) and at time t_k as

$$\begin{aligned} u_{ijk} &= \chi_{ijk}^T a \\ &= (\phi(x_i,y_i) \otimes \psi(z_j) \otimes \theta(t_k))^T a \end{aligned}$$

SYSTEM EQUATION

Once the interpolation functions are selected and the nonlinear material properties are approximated as explicit functions of position and time, one can proceed to integrate the terms in Eqs.42-43 to construct the equivalent matrices. The resultant finite element matrix equation for the time interval, I_n, can then be expressed as

$$\left[C_n(a_n)+K_n(a_n)+M_n^+(a_n)\right]a_n = q_n + \left[M_{n-1}^-(a_{n-1})\right]a_{n-1} + b_n \tag{46}$$

where the subscript, n, indicates that the associated matrix or vector is evaluated with functions defined in time interval, I_n. Note that each term in Eq.46 is corresponding to an integral in Eqs. 42-43, which can be evaluated based upon the interpolation functions of Eqs. 44-45. As an example, the capacitance matrix is given as

$$\begin{aligned} C_n &= \sum_p C_{\Omega_p} \\ &= \sum_p \int_{t_{n-1}}^{t_n} \left(\int_{\Omega_p} \rho c \frac{\partial u}{\partial t} w d\mathbf{x} \right) dt \end{aligned}$$

The details of an elemental capacitance matrix, C_{Ω_p} is given as Eq. A.1 in Appendix.

The matrix equation derived above is based upon the discontinuous Galerkin's method and will be solved in a time-marching fashion. In other words, the matrix equation of Eq. 46 will be solved for a time interval at a time, with a_n as unknown and a_{n-1} as known quantities. Because its nonlinear nature, Eq. 46 can be solved by the Newton-Raphson's method, which leads to a recursive formula

$$\left[C_n\left(a_n^{i-1}\right)+K_n\left(a_n^{i-1}\right)+M_n^+\left(a_n^{i-1}\right)+J_c(a_n^{i-1})+J_k(a_n^{i-1})+J_m(a_n^{i-1})\right]\Delta a_n^i = -R_n^{i-1} \tag{47}$$

and the solution is updated by

$$a_n^i = a_n^{i-1} + \Delta a_n^i \tag{48}$$

In the above equation, Δa_n^i is the improvement of the solution and R_n^{i-1} is the residual of the nonlinear equation at the i-1 iteration, which is defined as

$$R_n^{i-1} = \left[C_n\left(a_n^{i-1}\right)+K_n(a_n^{i-1})+M_n^+\left(a_n^{i-1}\right)\right]a_n^i - q_n - \left[M_{n-1}^-(a_{n-1})\right]a_{n-1} - b_n$$

Moreover, the derivative matrices, J_c, J_k and J_m are obtained by differentiating the coefficient matrices C_n, K_n and M_n^+ with respect to the unknown vector a_n, respectively. This is usually accomplished at the element level. As an example, the derivative matrix, J_c, is detailed in Appendix as Eq. A.2.

SENSITIVITY ANALYSIS

Since the matrix equation, Eq. 46 , is in the form of a static problem, $\boldsymbol{Ax=b}$. Differentiation of Eq. 46 with respect to a design variable, b, gives a sensitivity equation for a nonlinear transient heat transfer problem as,

$$(C + K + M^{+} + J_{c} + J_{k} + J_{M^{+}}).\frac{da_{n}}{db}$$

$$= -\left(\frac{dC}{db} + \frac{dK}{db} + \frac{dM^{+}}{db}\right)a_{n} + \frac{dM^{-}}{db}a_{n-1} + M^{-}\frac{da_{n-1}}{db} + \frac{dq}{db} \qquad (49)$$

The derivative matrices appearing in the right-hand side of Eq. 49 are new for sensitivity analysis. Generation of such matrices can be tedious and prone to mistakes. A typical derivative matrix, dC/db, is given in Appendix. Fortunately, because of the nature of approximation, those derivative matrices can be obtained in the same way as the original matrices themselves. This becomes evident by comparing Eqs. A1 and A3 in Appendix. Furthermore, it is noted that Eq. 49 is a linear equation of $\frac{da_{n}}{db}$, which enjoys the same left-hand side coefficient matrices as Eq. 46 . Thus, the factored matrices saved from the converged analysis, can be reused here to solve the sensitivity equation. That makes the sensitivity analysis computationally efficient.

NUMERICAL RESULTS

An academic example is used here to verify the derived equations. The space domain of the 2-D problem is a 1x1 square, which is discretized into two triangular p-version finite elements, as shown in Fig. 4. The heat source term, Q, is specifically selected so that the solution of the heat transfer problem, Eq.36, is

$$u_{e}(x, y, t) = xy(x-1)(y-1)t^{5}$$

which gives homogeneous boundary conditions and zero initial condition. Both the material properties, ρc and isotropic k, are assigned by a linear temperature relation,

$$\rho c, k = 20. + u$$

The time step is set to be 1 second and the total operational time, τ, is set to be 4 seconds.

In the numerical exercise, the orders of in-plane and the temporal polynomials are selected to be 4 and 6, respectively, for temperature interpolation, Eq. 44, whereas the orders of in-plane and the temporal polynomials are 3 and 5, respectively, for material property interpolation, Eq. 45. The total Lagrange points for the in-plane material interpolation is 10 as marked in Fig. 4. Moreover, the error is measured by the L^2-norm[15] as

$$\|e(t)\| = \left\{ \int_0^T \left[\int_\Omega \left[\left(\frac{\partial e}{\partial x}\right)^2 + \left(\frac{\partial e}{\partial y}\right)^2 + e^2 \right] dxdy \right] dt \right\}^{1/2}$$

where $e = u - u_e$ and u is the numerical solution.

At the end of the first time interval, $t_1 = 1$ second, the error is in the order of 10^{-4}. The error is growing with the time. At $t_2 = 2$ second, the error grows to the order of 10^{-1}. At $t_4 = 4$, the error becomes 13.31. The major source of the error is expected from deficiency in the in-plane interpolation of materials. The material property is linear in temperature. Thus, the exact order of in-plane material interpolation has to be 4 which is higher than 3, the order used in the current study. Such error will be accumulated from one time interval to the next. The results of temperature distribution are shown in Fig. 5.

Case 1

The slope of the thermal conductivity-temperature relation is considered as a design variable. Since only the matrix K depends upon this special design variable, the right-hand side of Eq.49 can be greatly reduced to a single term $-(dK/db)\boldsymbol{a}$. The results of the thermal sensitivity coefficients at times from 1 second to 4 seconds are shown in Fig. 6. Note that the thermal sensitivity coefficients is interpolated in the same way as the temperature; i.e.,

$$\frac{du}{db} = \chi^T(x,t)\frac{d\boldsymbol{a}}{db}$$

where $d\boldsymbol{a}/db$ is obtained from Eq. 49. Comparing with the finite differencing, the errors of the thermal sensitivity coefficients are less than 10^{-4} for all the time intervals. Note that in this example, thermal sensitivity analysis takes only 18% of the time required for one thermal analysis.

Case 2

Since in this study, the material property is a distributed function, one may then assume that the square slab is made of various materials. In this particular case, the value of k at each Lagrange point is determined by it's own material table. If the slope of each material table is considered as a design variable, there are 10 independent design variables in total. They are marked in Fig. 4.

Figures 7 and 8 show the thermal sensitivity coefficients of du / db_1 and du / db_9, where b_1 and b_9 are the slopes of the thermal conductivity-temperature relation at Lagrange points 1 and 9, respectively. The figures reveal that the design variable, b_1, effects the change of temperature along the diagonal line, whereas the design variable, b_9, does the area off the diagonal line more. Finally, all 10 thermal sensitivity coefficients of the temperature at the center point are collected and plotted out in Fig. 10. The picture indicates the degree of influence of individual design variable on the temperature at the center location at different time.

CONCLUSIONS

The paper uses two examples to demonstrate the derivation procedure for thermal sensitivity analysis. The continuous approach is used in the first example and the discrete approach is used in the second example. It is shown in the first example that the direct differentiation method can achieve better accuracy in thermal sensitivity analysis than the adjoint variable method. Several authors have similar observation. Furthermore, Example 1 shows that the direct results of the direct differentiation method, thermal derivatives of the temperature, are very useful in design. This particular advantage of the direct differentiation method is also demonstrated in Example 2.

The second example presented here only represented an initial attempt to find the thermal sensitivity based upon the p-version time-discontinuous Galerkin's method. Though construction of the matrix equation for thermal analysis is complicated, construction of that for thermal sensitivity analysis is rather simple. The resultant sensitivity equation is also demonstrated to be computationally efficient. However, more works are needed to develop error-control capability for thermal analysis and sensitivity analysis to ensure the quality of the p-version time-discontinuous Galerkin's method.

ACKNOWLEGDE:

This work is supported by NASA Langley Research Center under Grant NAG-1-2300. Many beneficial discussions with Dr.Kim Bey at NASA Langley Research Center and Professor Hideaki Kaneko at Old Dominion University are greatly appreciated.

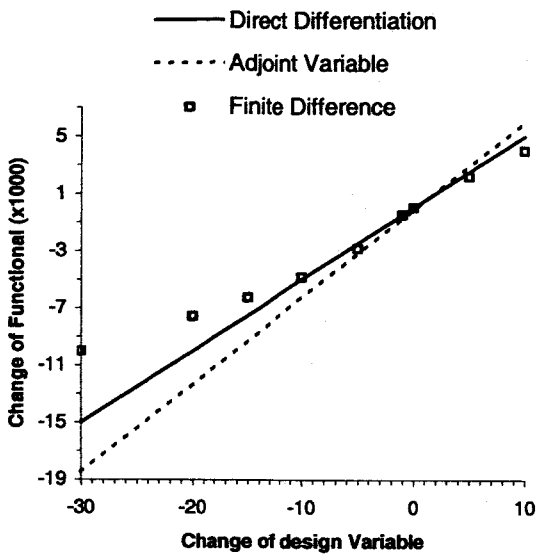

Figure 1: Thermal Design Derivatives for Press Molding with Respect to the Mold Temperature.

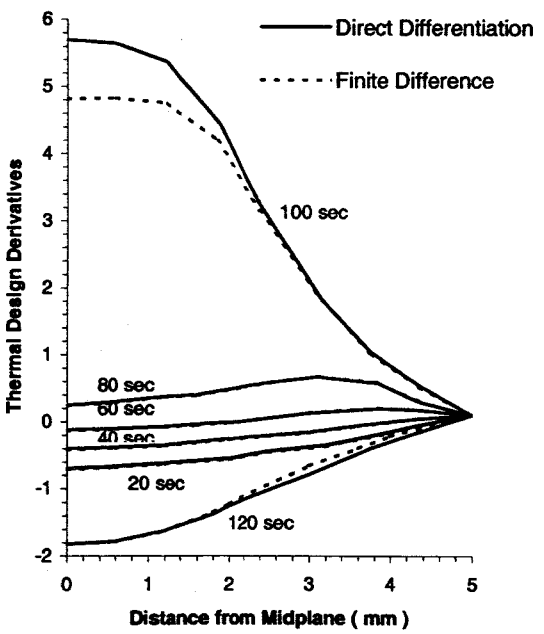

Figure 2: Profiles of Thermal Design Derivatives of Temperature with Respect to the Mold Temperature.

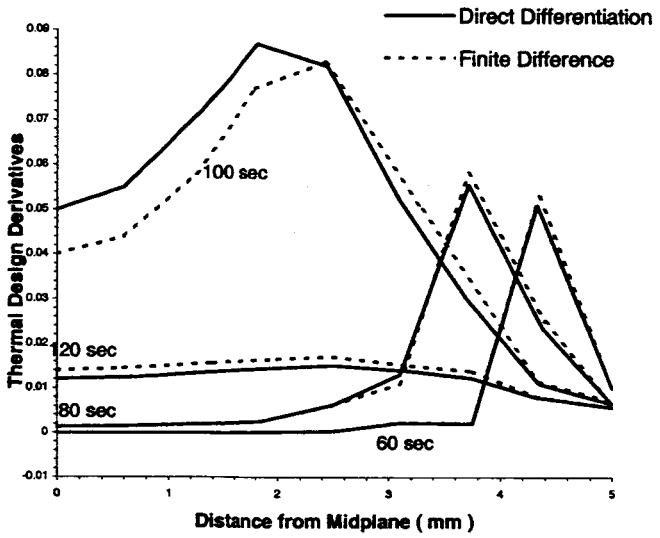

Figure 3: Profiles of Thermal Design Derivatives of the State of Cure with Respect to the Mold Temperature.

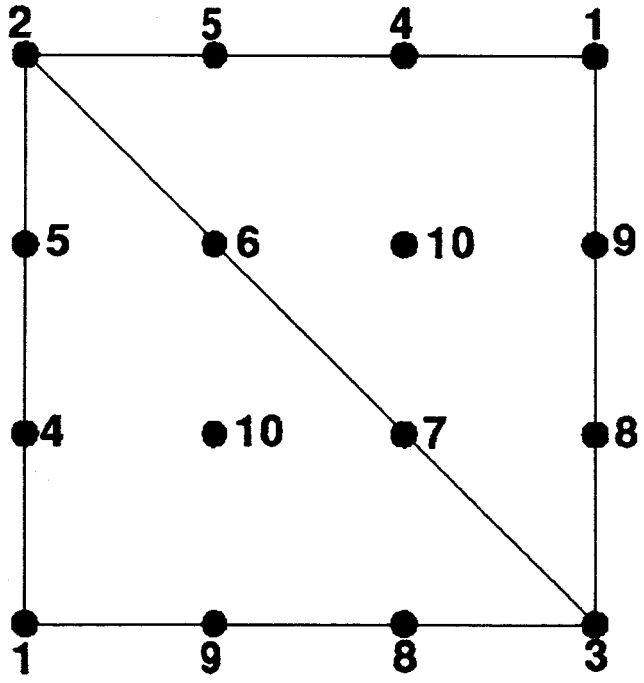

Figure 4: Meshes and Lagrange Points for Interpolation of Material Property

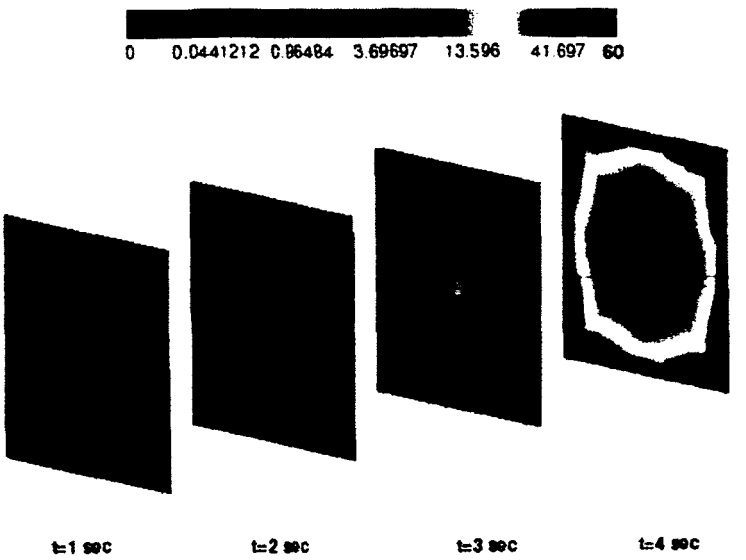

Figure 5: Temperature Distribution

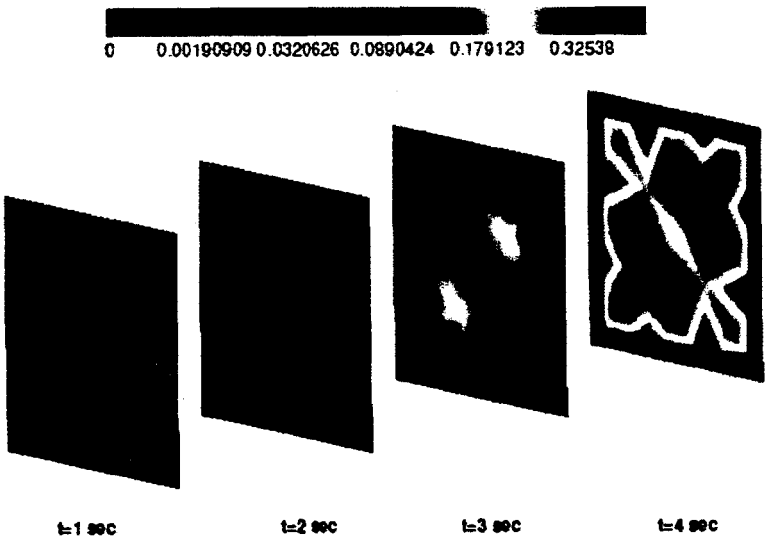

Figure 6: Coefficients of Thermal Sensitivity with Respect to Homogeneous Thermal Conductivity; $\frac{\partial u(x,y)}{\partial b}$.

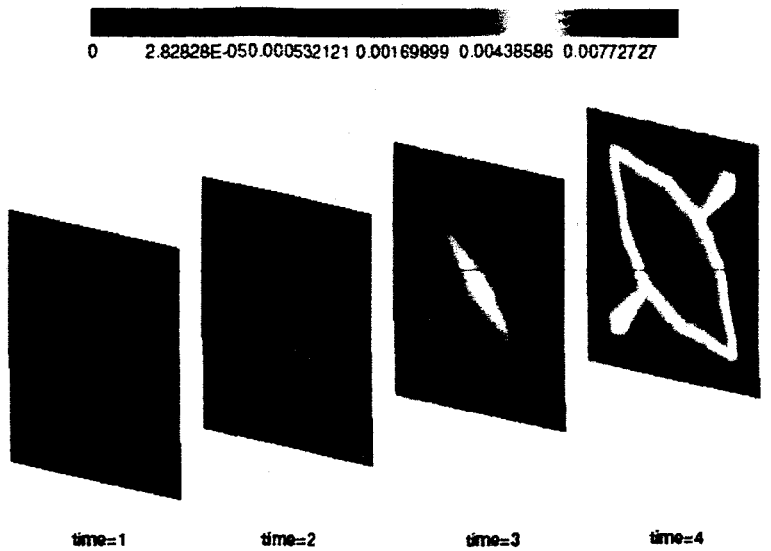

Figure 7: Coefficients of Thermal Design Sensitivity with Respect to Thermal Conductivity at Material Lagrange Point 1; $\frac{\partial u(x,y)}{\partial b_1}$.

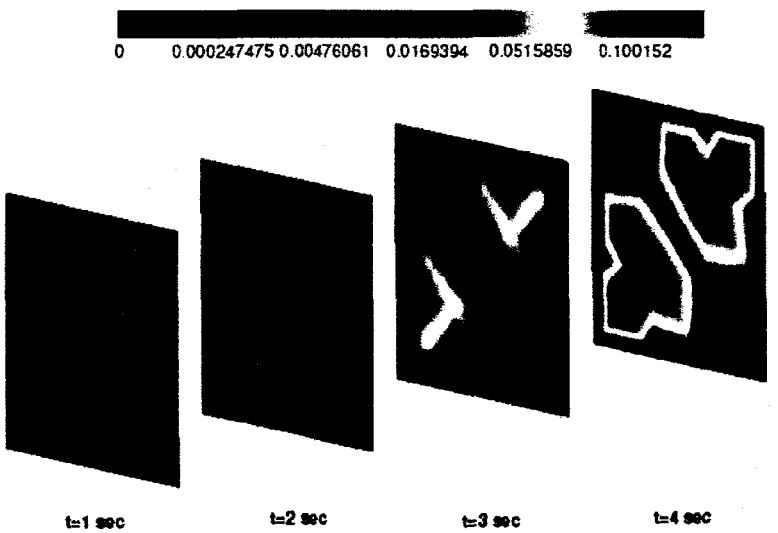

Figure 8: Coefficients of Thermal Design Sensitivity with Respect to Thermal Conductivity at Material Lagrange Point 9; $\frac{\partial u(x,y)}{\partial b_9}$.

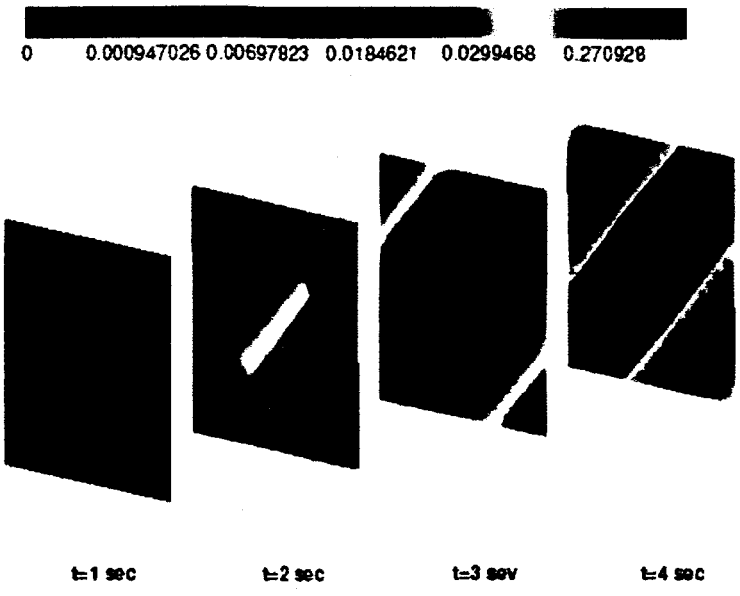

Figure 9: Coefficients of Thermal Design Sensitivity with Respect to Thermal Conductivity; $\frac{\partial u(x_c, y_c)}{\partial b_i}$; i =1 to 10.

REFERENCES

1. Sherman, L. L., Taylor, A. C. III, Green, L. L., Newman, P. A., Hou, G. J-W., and Korivi, V. M., "First- and Second-Order Aerodynamic Sensitivity Derivatives via Automatic Differentiation with Incremental Iterative Methods," *Journal of Computational Physics*, Vol. 129,1996, pp.307-331.
2. Newman, J. C. III, Whitfield, D. L. and Anderson, W. K., "Step-Size Independent Approach for Multidisciplinary Sensitivity Analysis, " *AIAA Journal*, Vol. 40, No. 3, 2003, pp. 566-578.
3. Haug, E. J., Choi, K. K. and Komkov, V., *Design Sensitivity Analysis of Structural Systems,* Academic Press, 1985.
4. Haftka, R. T. and Gurdal, Z., *Elements of Structural Optimization*, Kluwer Academic Publishers, Third Edition, 1992.
5. Tortorelli, D. A. and Michaleris, P., "Design Sensitivity Analysis; Overview and Preview," *Inverse Problem in Engineering*, Vol. 1, pp. 71-103, 1994.
6. Adelman, H. M., Haftka, R. T., Camarda, C. J., and Walsh, J. L., "Structural Sensitivity Analysis: Methods, Applications and needs," NASA TM-85827, June 1984.
7. Haftka, R. T., "Techniques for Thermal Sensitivity Analysis," *International Journal of Numerical methods in Engineering*, Vol. 17, No. 1, 1981, pp. 71-80.
8. Hou, J. W. and Sheen, J. S., "Numerical Studies of he Design Sensitivity Calculation for a Reaction-Diffusion System with Discontinuous Derivatives," *Engineering Optimization*, Vol.11, 1987, pp.103-119.

9. House, J. M.,Arora, J. S., Smith, T. F., "Comparison of Methods for Design Sensitivity Analysis for Optimal Control of Thermal Systems," *Optimal Control Application and Methods*, Vol. 14, No. 1,1993, pp.17-37.
10. Suresha, S. and Gupta, S. C., "Transient Thermal Sensitivity Analysis during Solar Eclipse with Discontinuous Heat Load," *Journal of Spacecraft and Rockets*, Vol. 36, No. 6, 1999, pp.916-918.
11. Suresha, S., Gupta, S. C. and Katti, R. A., "Thermal Sensitivity Analysis of Spacecraft Battery," *Journal of Spacecraft and Rockets*, Vol. 34, No. 3, 1997, pp.384-390.
12. Lee, S. H. and Albright, C. E., "Thermal Sensitivity Analysis by Use of an Analytic Solution for Laser Surface Treatment," *Journal of Physics D: Applied Physics*, Vol. 35, 2002, pp.710-715.
13. Tortorelli, D. A., Haber, R. B., and Lu, S. C.-Y., "Design Sensitivity Analysis for Nonlinear Thermal Systems," *Computer Methods in Applied Mechanics and Engineering*, Vol. 77, Dec. 1989, pp. 61-77.
14. Smith, D. E.,"Design Sensitivity Analysis and Optimization for Polymer Sheet Extrusion and Mold Filling Process," *International Journal for Numerical Methods in Engineering*, Vol. 57, 2003, pp.1381-1411.
15. Tomey, J. P., "The *p*-Version Discontinuous Galerkin Method for Heat Transfer in Built-up Structures," M.S. Thesis, George Washington University, May, 2001.
16. Walker, D. T., "Nonlinear Conduction Heat Transfer Using a Hierarchical Finite Element Method," M.S. Thesis, George Washington University, June, 2003.
17. Kaneko, H.. and Bey, K. S., "Error Analysis of *p*-Version Discontinuous Galerkin Method for Heat Transfer in Built-up Structures," (in preparation)
18. Barone, M. E., and Caulk, D. A., "The Effect of Deformation and Thermoset Cure on Heat Conduction in a Chopped-Fiber Reinforced Polyester during Compression Molding," *International Journal Heat Mass Transfer,* Vol. 22, 1979, pp. 1021-1032.
19. Hou, G J.-W., Hou, T.-H. and Sheen, J. S., "Optimal Cure Cycle Design for the Fiber Reinforced Composite Lamination Processing", *The Journal of International Polymer Processing,* Vol. 5, No. 2, 1990, pp. 88-99.
20. Shampine, L. F. and Gordon, M. K., *Computer Solution of Ordinary Differential Equations: The Initial Value Problem*, W. H. Freeman and Co., San Francisco, 1975.
21. Szabo, B., Babuska, I., *Finite Element Analysis*, John Wiley & Sons, New York, 1991.

APPENDIX:

$$C_{\Omega_e} = \int_{t_{n-1}}^{t_n} \int_{\Omega_p} \int_{\frac{-d}{2}}^{\frac{d}{2}} \rho c \chi \frac{\partial \chi^T}{\partial t} dz dA dt$$

$$= \int_{t_{n-1}}^{t_n} \int_{\Omega_e} \int_{\frac{-d}{2}}^{\frac{d}{2}} (N_c^T \delta_c)(\varphi \otimes \psi \otimes \theta)\left(\varphi \otimes \psi \otimes \frac{d\theta}{dt}\right)^T dz dA dt \qquad \text{(A.1)}$$

$$= \sum_i \sum_j \sum_k \{(\int_{\Omega_p} \varphi \varphi^T N_{cpi} dA \otimes \int_{\frac{-d}{2}}^{\frac{d}{2}} \psi \psi^T N_{czk} dz \otimes \int_{t_{n-1}}^{t_n} \theta \frac{d\theta^T}{dt} N_{ctj} dt)\delta_{ijk} \}$$

$$J_{c,\Omega_p} = \int_{t_{n-1}}^{t_n} \int_{\Omega_p} \int_{\frac{-d}{2}}^{\frac{d}{2}} \frac{\partial(\rho \rho c}{\partial a}(\chi) \frac{\partial(\chi^T \cdot a)}{\partial t} dz dA dt$$

$$= \int_{t_{n-1}}^{t_n} \int_{\Omega_p} \int_{\frac{-d}{2}}^{\frac{d}{2}} N_c^T \frac{\partial \delta_c}{\partial a}(\varphi \otimes \psi \otimes \theta)\left(\varphi \otimes \psi \otimes \frac{d\theta}{dt}\right)^T a dz dA dt \qquad \text{(A. 2)}$$

$$= \sum_i \sum_j \sum_k \{[(\int_{\Omega_p} \varphi \varphi^T N_{cpi} dA \otimes \int_{\frac{-d}{2}}^{\frac{d}{2}} \psi \psi^T N_{czk} dz \otimes \int_{t_{n-1}}^{t_n} \theta \frac{d\theta^T}{dt} N_{ctj} dt)a](\alpha_{ijk} \chi_{ijk})\}$$

$$\frac{dC_{\Omega_p}}{db} = \int_{t_{n-1}}^{t_n} \int_{\Omega_p} \int_{\frac{-d}{2}}^{\frac{d}{2}} \frac{\partial(\rho c)}{\partial b} \chi \frac{\partial \chi^T}{\partial t} dz dA dt$$

$$= \int_{t_{n-1}}^{t_n} \int_{\Omega_e} \int_{\frac{-d}{2}}^{\frac{d}{2}} (N_c^T \frac{\partial \delta_c}{\partial b})(\phi \otimes \psi \otimes \theta)\left(\phi \otimes \psi \otimes \frac{d\theta}{dt}\right)^T dz dA dt \qquad \text{(A.3)}$$

$$= \sum_i \sum_j \sum_k \{(\int_{\Omega_p} \phi \phi^T N_{cpi} dA \otimes \int_{\frac{-d}{2}}^{\frac{d}{2}} \psi \psi^T N_{czk} dz \otimes \int_{t_{n-1}}^{t_n} \theta \frac{d\theta^T}{dt} N_{ctj} dt) \frac{\partial \delta_{ijk}}{\partial b} \}$$

Attachment II

Fortran Source Code and Sample Input Data Files

The files saved on the attached CD are listed below.

1. *README.txt* – Short Explanation of the attached FORTRAN Files

2. *schtmain6.f* – the main source code based upon the *p*-version Galerkin's method for a 3D nonlinear, transient heat conduction problem.

3. *input3dn6.dat* – connectivity information for elements in time and through-thickness, the tabulated data for material properties

4. *joint_input.dat* – connectivity information for elements in xy plane

5. *q3dt5z1xy4_pt6_pxy4_pz6nl.dat* – input of thermal load vector which is obtained based upon the exact solution given by Eq.(20)